THESIS FOR THE DEGREE OF DOCTOR OF PHILOSOPHY

Conjoined piezoelectric harvesters and carbon supercapacitors for powering intelligent wireless sensors

HENRIK STAAF

Department of Microtechnology and Nanoscience
CHALMERS UNIVERSITY OF TECHNOLOGY

Göteborg, Sweden 2018

Conjoined piezoelectric harvesters and carbon supercapacitors for powering intelligent wireless sensors

HENRIK STAAF

Micro and Nanosystems group
Electronics and Materials Systems Laboratory
Departement of Microtechnology and Nanoscience
Chalmers University of Technology
SE-412 96 Göteborg, Sweden
Tel. +46-(0)31 772 10 00

COVER: Energy sources for intelligent wireless sensors; from idea, blueprint to reality

Conjoined piezoelectric harvesters and carbon supercapacitors for powering intelligent wireless sensors

HENRIK STAAF

Departement of Microtechnology and Nanoscience

Chalmers University of Technology

Abstract

To achieve total freedom of location for intelligent wireless sensors (IWS), these need to be autonomous. To achive this today there is a need of broadband piezoelectric energy harvesting and a long-lasting energy. The Harvester need to be able to provide sufficient amount of energy for the intelligent wireless sensor to perform its task. The energy storage needs to fulfill the requirement of a large number of charge discharge cycles and contain sufficient power for the intelligent wireless sensor.

The biggest issue with piezoelectric energy harvesting today is the bandwidth limitation. Solutions today to achieve larger bandwidth make a tradeoff where the output is decreased. The biggest issue for energy storage today is the limitation of energy density for supercapacitors and the lack of sufficient life cycles for batteries.

This thesis aims to realize piezoelectric energy harvesters with broad bandwidth and maintained power output. Moreover, for energy storage in the form of supercapacitors realize an electrode material that has a high effective surface area, good conductivity not dependent on a conductive agent and can be used without a binder. This thesis cover background and history of the two fields, discussion of technologies used and presents solutions for piezoelectric energy harvesting and carbon based supercapacitor storage.

A Backfolded piezoelectric harvester was made of two conjoined piezoelectric cantilevers, one placed on top of a bottom cantilever. By the backfolded design this thesis show that by utilizing the extended stress distribution of the bottom cantilever a maintained power output is achieved for both output peaks. By introducing asymmetry where the top cantilever have 80% length compared with the bottom cantilever the bandwidth was increased. An effective bandwidth of 70 Hz with voltage output above 2,75 V for 1 g is achieved.

To achieve further enhanced bandwidth a piezoelectric energy harvester with selftuning was designed. The selftuning was achieved by a sliding mass on a beam, which is conjoined, to two piezoelectric cantilevers in a backfolded structure. By introducing length asymmetry, the effective bandwidth was enhanced to 38 Hz with a power output above 15 mW, for 1 g, which is sufficient for an intelligent wireless sensor to start up and transmit data.

To utilize the positive output effect from conjoined cantielvers a micro harvester was fabricated. The design was based on the same principle as for the backfolded, but for fabrication reasons the design was made in one plane. The harvester contain two outer cantilevers conjoined to a backfolded middle cantilever. Due to fabrication difficulties, only a mechanical characterization of the harvester was possible. The result from the characterization looks promising from a harvesting point of view, by showing a clear peak that seems to be somewhat broadband.

Energy storage for an autonomous wireless intelligent sensor (IWS) needs to be able to charge and discharge during the lifetime of the IWS. Therefor the choice fell on supercapacitors instead of batteries. Over time the supercapacitor due to its superior amount of charge and discharge cycles, outperform a battery when energy density is compared.

Increasing the energy density for supercapacitors gives the advantage to prolong the providing of power to the IWS. One such electrode material is conjoined carbon nanofibers and carbon nanotubes. The material is not dependent on conductive agents or binders. The effective surface area can be expanded through a denser structure of CNF, where more CNT can grow. In combination with activation, which will yield more micropores, hence an increased capacitance for the presented synthesized material yielded 91 F/g with an effective surface area of 131 m^2.

There is many challenges to power an IWS on a gasturbine. This thesis cover challenges like vibrations on cables, placement issues and the charge of a supercapacitor by harvested energy that comes in small chunks. Solutions for these challenges are offered.

The presented work in this thesis shows how the bandwidth for piezoelectric energy harvesters can be broader by asymmetric implementation of conjoined resonators. In addition, the advantages of conjoined carbon electrode materials to be implemented as electrode material in supercapacitors. Both harvester and storage are intended to be used as energy sources for intelligent wireless sensors.

Keywords: Intelligent wireless sensor, Supercapacitor, electrode material, carbon nanomaterials, Kinetic harvesting, piezoelectric energy harvesting, selftuning, coupled resonators

"A parent's energy is harvested in full from the one given by their children"
To Nelly & Noah

List of appended papers

This thesis is based on the work in the following appended papers:

Paper I
SIMULATION AND EXPERIMENTAL DEMONSTRATION OF IMPROVED EFFICIENCY IN COUPLED PIEZOELECTRIC CANTILEVERS BY EXTENDED STRAIN DISTRIBUTION
L G H Staaf, E. Köhler, D. Parthasarathy, P Lundgren and P Enoksson
Sensors Actuators A Phys., vol. 229, pp. 136–140, 2015

Paper II
IMPACT OF DESIGNED ASYMMETRIES ON THE EFFECTIVE BANDWIDTH OF A BACKFOLDED PIEZOELECTRIC ENERGY HARVESTER
L G H Staaf, A Smith, E. Köhler, P D Folkow, P Lundgren and P Enoksson
Submitted

Paper III
ACHIEVING INCREASED BANDWIDTH FOR 4 DEGREE OF FREEDOM SELF-TUNING ENERGY HARVESTER
L G H Staaf, A Smith, E Köhler, P D Folkow, P Lundgren and P Enoksson
J. Sound Vib., vol. 420, pp. 165–173, 2018

Paper IV
EFFECTIVE PIEZOELECTRIC ENERGY HARVESTING BANDWIDTH ENHANCEMENT BY ASSYMETRY AUGMENTED SELF-TUNING OF COUPLED CANTILEVERS
L G H Staaf, A Smith, P D Folkow, P Lundgren and P Enoksson
Submitted

Paper V
A MICRO-MACHINED COUPLED-CANTILEVER FOR PIEZOELECTRIC ENERGY HARVESTERS
A Vyas, L G H Staaf, C Ruso, T Ebefors, J Liljeholm, AD Smith, P Lundgren and P Enoksson
Micromachines 2018, 9(5), 252; https://doi.org/10.3390/mi9050252

Paper VI
PRESENT AND FUTURE SUPERCAPACITOR CARBON ELECTRODE MATERIALS FOR IMPROVED ENERGY STORAGE USED IN INTELLIGENT WIRELESS SENSOR SYSTEMS
L G H Staaf, P Lundgren and P Enoksson
Nano Energy, vol. 9, pp. 128–141, 2014

Paper VII
HIERARCHICAL CELLULOSE- DERIVED CNF/CNT COMPOSITES FOR ELECTROSTATIC ENERGY STORAGE
V Kuzmenko, A M Saleem, L G H Staaf, M Haque, A Bhaskar, M Flygare, K Svensson, V Desmaris and P enoksson
J. Micromechanics Microengineering, vol. 26, no. 12, 2016

Paper VIII
PIEZOELECTRIC ENERGY HARVESTING AS ENERGY SOURCE FOR AUTONOMOUS INTELLIGENT WIRELESS SYSTEMS ON GAS TURBINES
L G H Staaf, E Köhler, J Kemp, M Allen, S Zenkic, A Lindblom, M Christodoulou, J Roberts, P Lundgren and P Enoksson
EVI-GTI and PIWG Joint Conference on Gas Turbine Instrumentation, 2016, p. 4 (17 .)-4 (17 .)

Papers not included due to overlap or being outside scope of this thesis:

CAPACITIVE EFFECTS OF NITROGEN DOPING ON CELLULOSE-DERIVED CARBON NANOFIBERS
Volodymyr Kuzmenko, Olga Naboka, Henrik Staaf et al
Journal of Materials Chemistry and Physics. Vol. 160, p. 59-65

HIGH TEMPERATURE ENERGY HARVESTER FOR WIRELESS SENSORS
Elof Köhler, Richard Heijl, Henrik Staaf et al
Journal of Smart Materials and Structures. Vol. 23 (9), p. Art. no. 095042-

SUSTAINABLE CARBON NANOFIBERS/NANOTUBES COMPOSITES FROM CELLULOSE AS ELECTRODES FOR SUPERCAPACITORS
Volodymyr Kuzmenko, Olga Naboka, Mohammad Mazharul Haque, Henrik Staaf et al
Journal of Energy. Vol. 90 (2), p. 1490-1496

VERIFICATION OF SELF-TUNING 4DOF PIEZOELECTRIC ENERGY HARVESTER WITH ENHANCED BANDWIDTH
Henrik Staaf, Elof Köhler, Anderson David Smith et al
PowerMEMS 2017, The 17th international conference on Micro and Nanotechnology for Power Generation and Energy Conservation Application, November 14-17, Kanazawa, Japan

SELFTUNING ENERGY HARVESTER BY SLIDING WEIGHT
Henrik Staaf, Elof Köhler, Peter Folkow et al
Svenska Mekanikdagarna 2017, 12-13 juni, Uppsala, Sverige

MINIATURIZED SUPERCAPACITORS FOR SMART SYSTEMS
Qi Li, Volodymyr Kuzmenko, Mohammad Mazharul Haque, Henrik Staaf et al
Smart Systems Integeration 2017, 8 - 9 March, Cork, Ireland

SMART DESIGN PIEZOELECTRIC ENERGY HARVESTER WITH SELF-TUNING
Henrik Staaf, Elof Köhler, Peter Folkow et al
Journal of Physics: Conference Series. Vol. 922 (1)

NANOCOMPOSITE MATERIALS FOR MINIATURIZED SUPERCAPACITORS
Qi Li, Volodymyr Kuzmenko, Mohammad Mazharul Haque, Henrik Staaf et al
International Conference and Exhibition on Integration Issues of Miniaturized Systems 2017, SSI 2017, Cork, Ireland, 8-9 March 2017, p. 199-205

SUPERCAPACITOR WITH INCREASED CAPACITANCE AT 200°C
Elof Köhler, Henrik Staaf, Peter Enoksson
IET Conference Publications. EVI-GTI and PIWG Joint Conference on Gas Turbine Instrumentation; Berlin; Germany; 27-29 September 2016 (CP693)

PROOF OF CONCEPT THERMOELECTRIC ENERGY HARVESTER POWERING WIRELESS SENSOR ON GAS TURBINE
Elof Köhler, Henrik Staaf, J. Kemp et al
EVI-GTI and PIWG Joint Conference on Gas Turbine Instrumentation, Berlin, Germany, 27-29 September 2016 (CP693)

CARBON NANOTUBES/NANOFIBERS COMPOSITES FROM CELLULOSE AS ELECTRODES FOR SUSTAINABLE ENERGY DEVICES
Volodymyr Kuzmenko, Muhammad Amin, Olga Naboka, Henrik Staaf et al
The World Conference on Carbon (Carbon2014), June 29 - July 4, Jeju, South Korea. Vol. ORT6-54

NITROGEN-DOPED CARBON NANOFIBERS SYNTHESIZED FROM ELECTROSPUN CELLULOSE AS SUPERCAPACITOR ELECTRODE
Volodymyr Kuzmenko, Henrik Staaf, Olga Naboka et al
2nd International Conference on Materials for Energy May 12-16, 2013

CARBON NANOTUBES AS ELECTRODE FOR SUPERCAPACITORS
Henrik Staaf, Muhammad Amin, Gert Göransson et al
2nd International Conference on Materials for Energy, May 12-16, 2013 and Karlsruhe, Germany

FABRICATION OF HIGH TEMPERATURE THERMOELECTRIC ENERGY HARVESTERS FOR WIRELESS SENSORS
Elof Köhler, Richard Heijl, Henrik Staaf et al
Journal of Physics: Conference Series. Vol. 476 (1), p. Art. no. 012036-

FUTURE ELECTRODE MATERIALS FOR SUPERCAPACITORS IN INTELLIGENT WIRELESS SENSOR SYSTEM
Henrik Staaf, Peter Enoksson, Per Lundgren
MME 2012, Micromechanics and Microsystems Europe Workshop September 9 - 12, 2012, Ilmenau, Germany

Acknowledgements

If you read these lines, you are among those who I owe gratitude for what I have achieved during these last years. There are many important people who I owe and I hope that I have not forgotten anyone.

Peter Enoksson my supervisor for whom nothing is impossible and problems are only obstacles towards solutions. Your creativity seems endless as your hunger for knowledge. Thanks for all the inspiration and knowledge you given me so far. Also thanks for all technical, historical discussions and for being a nice travel companion. In addition, not to mention an airplane flight I will not forget.

Per Lundgren for all your good advices and endless feedback on my work. Moreover, during that work path, showing me that whatever happens, there is always something positive to learn from it. I also had many pleasant discussions over the years regarding board games and roleplaying games, which I hope to continue.

Peter Folkow for being a very good discussion partner regarding imaginative beam structures and for always creating a nice discussion environment, not only for science topics but also topics of life in general.

Kristina Rusu for being a very good collaboration partner in science projects and a happy travel companion on conferences.

My roomies; Sofia, Volodymyr and Agin for all the fun discussions and the nice environment we have.

Elof Köhler, for being a nice travel companion, laboratory third hand and all our discussions regarding food, computers and games (and of course all the scientific progress and discussions).

Thanks to Olga, Mazharul, Qi, Andersson and other colleges in the group over the years, for making a good working environment.

The workshop; Mats Myremark and Lars Jönsson for all help with realizing my harvesting gadgets, thank you.

Sanel Zenkic, Anders Lindblom and Edvard Svenman at GKN Aerospace, James Roberts at Rolls Royce PLC®, John Kemp and Michael Allen at Coventry University and Marios Christodoulou at SCITEK consultants LTD for a great collaboration in the gas turbine laboratories as well as pleasant company outside the labs and on conferences.

Ellen Lindqvist, Erik Isakson and Anna Kohlström, at IT-gymnasiet Göteborg, for being exemplary good executives when working half time in two places, which sometime is a great challenge and unorthodox solutions are needed.

To my parents, Solvig and Olle and to my brother in law Jens and my sister Annika, who asks questions about my research and your support, thank you.

Last but not the least, my family. My children Nelly and Noah for all questions about my research, including hilarious word shift regarding voltage. Which in Swedish (spänning) can be both voltage and excitement. Their support during dark days when the wind blows towards oneself, the sun is not shining and research not going in the direction expected… you have always been there with cheers and encouragement. My beloved wife Ellen, for your endless patience with all my projects and me (pointing all over me). Words are not enough to express my deepest gratitude for your invaluable support, so I will refrain from forcing them ♥ .

<div style="text-align: right;">Lindome, oktober 2018</div>

<div style="text-align: right;">Henrik Staaf</div>

TABLE OF CONTENTS

INTRODUCTION

1.1 BACKGROUND

When autonomous intelligent wireless sensors are mentioned, you may start thinking about advanced technical gadgets equipped with AI, like a drone able to perform tasks. But back in time, in a way, the first intelligent wireless sensor node was a beacon with a scout on a peak at a coastline. Set up in a network along the coast, these beacons when lit, were warning people of approaching enemies. In this ancient case, we the humans, where the autonomous intelligent sensor and the beacon was acting as a transmitting system and put together with a chain of beacons the direct translation for today would be an intelligent wireless sensor network. Imagine that these scouts stood there for hours, days, weeks, months looking at the horizon. Surveying from the coastline, waiting, and if they saw a ship had to decide if it was a friendly or a hostile, using optical sensors, the eyes. This was not a one man task, since it was very tedious and sleep is needed, a number of men had to be assigned to each beacon. It took humanity until recently, when wireless sensors started to be used as forest fire detectors [1], [2] to replace humans as overseers. Solutions for autonomous wireless sensors by energy harvesting windmills are investigated [3] to make these nodes completely autonomous. These fire detectors have the ability to cover a huge area and replace human watchtowers and video surveillance, making it more cost efficient and easier to oversee.

Further, intelligent wireless sensor systems are beginning to be used to monitor numerous things in our surroundings. Where an intelligent wireless sensor (IWS) gathers data, processes the data and transmits the result to a monitoring device. Together with an energy harvester converting ambient energy to electricity it becomes an IWS system that can work autonomously [4]–[9]. Being able to monitor the health of buildings [10], structures [11], machines [12], human body [13], conditions of roads [14] etc. (Figure 1.1). Will have a positive impact on our lives, since with more efficient monitoring, energy consumption can be reduced. Examples of this are the warming and cooling of houses [15] and fuel consumption for example airplanes [16], which properly monitored and controlled will use less energy resources and will generate less pollution.

Today we are mostly limited by the quantity and length of cables that have to be used for the sensors, or the lifetime of batteries, which have to be replaced in IWS. These boundaries limiting the possibilities to place a sensor or an IWS anywhere, to be operational for a very long time [17].
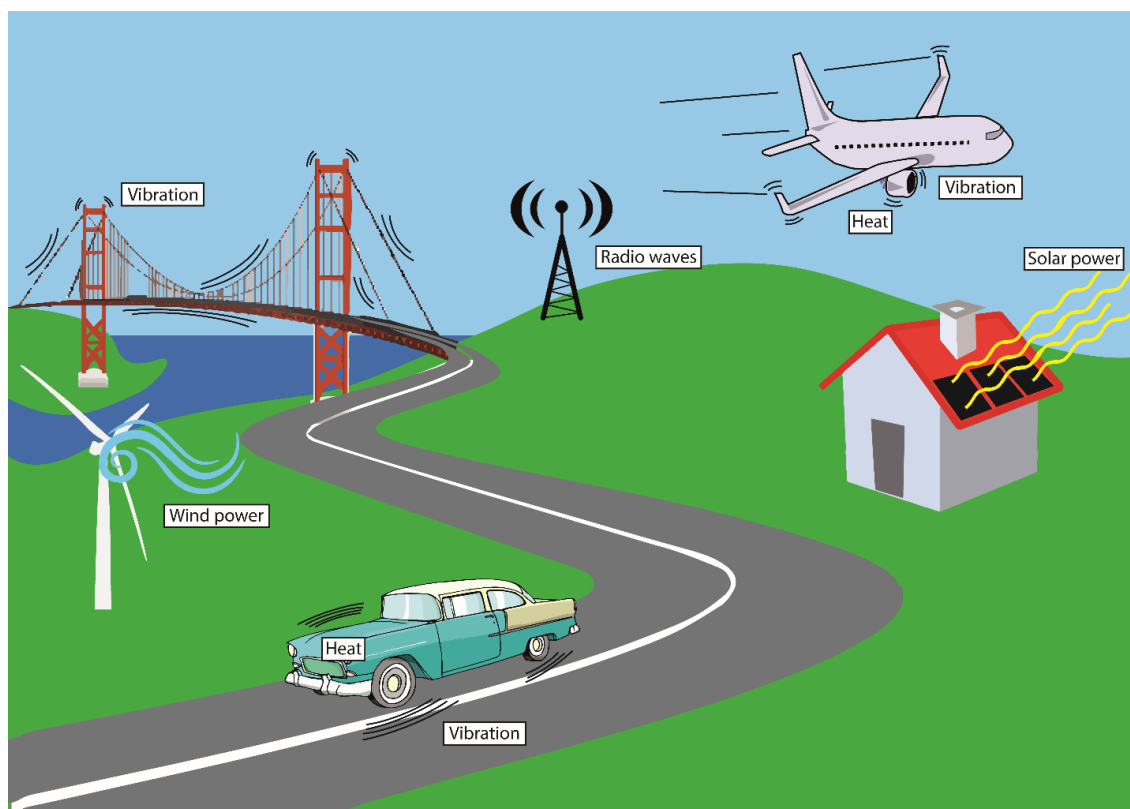
Figure 1.1 An overview of different possible ambient energy sources available for energy harvesting to provide power to Intelligent wireless sensor systems

One of the main challenges for IWS systems is the power consumption where a great deal of research has been done over the last years to compress the transmitting data, hence consume less power [18]. Also, progress in low power circuits technology makes it easier to craft IWS systems for more applications. Despite these efforts, 2-3 mW is used to transmit data wirelessly [19], [20]. The wireless transmission is not usually continuous but occurs in intervals while the energy harvester scavenges energy to be used for the transmissions. An even bigger challenge is the powering of the startup sequence for the wireless transmitter which consumes most power about 8-240 mW [21], which is far from reachable directly for most harvesters today. Therefore, a smart power manager has to be used combined with a storage device, that first store the energy and then release enough energy for first the startup sequence of the RF interface and then supply enough power for the RF interface to be able to send data intermittent.

For more data and further accurate data reading numerous IWS are connected in a network called a wireless sensor network (WSN). By using many IWS in a WSN the readings get more accurate and the IWS can transfer data between each other and do not have to have a direct connection to the gateway (Figure 1.2) [22].
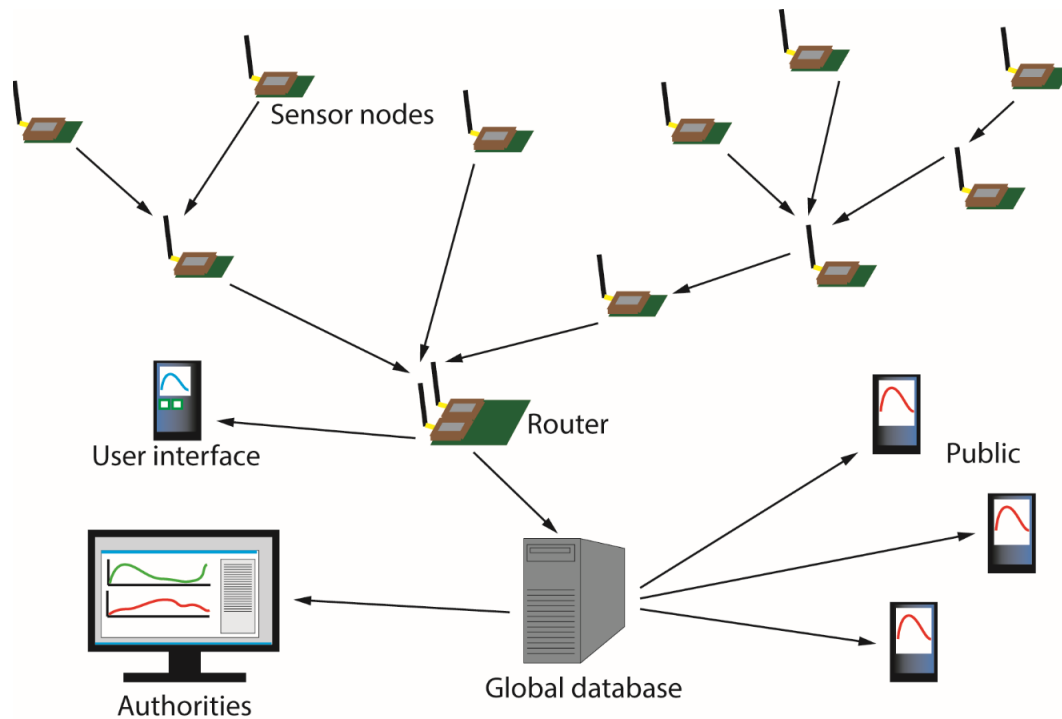
Figure 1.2, A setup of sensors in a wireless sensor network, where data is forwarded towards a gateway (router) and the data can be accessed by public users and surveyed by authorities.

1.2 SCOPE AND OUTLINE

The scope and outline of this thesis is to investigate power sources for intelligent wireless sensors, primarily on gas turbines. These power sources are divided into energy storage and energy harvesting.

In chapter 1, intelligent wireless sensor systems are described, including an overview of the components that such a system contains; energy storage and energy harvesting solutions for these systems are presented.

In chapter 2, piezoelectricity and its mechanism and how to harvest energy with a piezoelectric harvester are described. The development of novel designs with conjoined cantilevers for a piezoelectric harvester to be used for a gas turbine sensor application is presented (Figure 1.3, Paper I – V). The impact of a conjoined design with two cantilevers is investigated for further improvement in power output and for reaching a wider bandwidth. A micro harvester with conjoined cantilevers in one plane is also presented.

In chapter 3, supercapacitors are presented. The background theory and the specifications of electrode materials for supercapacitors used in IWS systems are presented. Results from recent research on carbon allotropes as electrode material are presented and evaluated to find a way

towards new and better electrode material (Paper VI). Further is a conjoined carbon electrode material based on CNFs and on CNTs grown on CNFs presented (Paper VII).

In chapter 4, measurements in an authentic commercial test environment on a gas turbine is presented along with a discussion on remaining challenges and potential solutions (Paper VIII).

The 5th and final chapter comprises discussion, conclusion and suggestions for future work based on the results from previous chapters in the thesis.
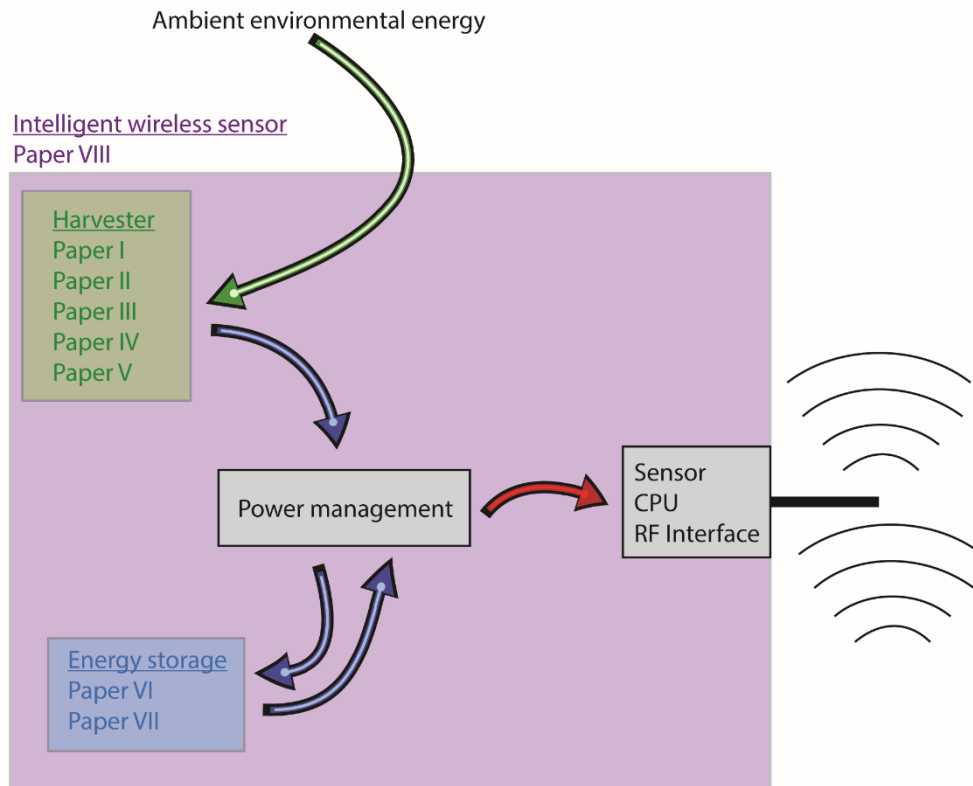
Figure 1.3, Schematic of an intelligent wireless sensor and its components. Presented is also the research areas for this thesis, marked as Paper I – VIII.

1.3 COMPONENTS OF AN INTELLIGENT WIRELESS SENSOR SYSTEM

An autonomous intelligent wireless sensor (AIWS) system is assembled from different components and needs an ambient source of energy. The IWS itself holds the sensor, CPU and RF interface. Where the sensor is used for collecting nearby data that the central processor unit (CPU) will process, and the RF interface sends and receives data. A power manager distributes the energy between the sensor, the CPU, the RF interface and the energy storage. For the AIWS system, a harvester is added, that will harvest enough energy for the AIWS to start up and manage its dedicated task (Figure 1.3).

1.3.1 DC converter and power manager

The harvested energy that is converted into electricity often comes in the form of an AC signal, while low power circuits needs a DC power supply. The input AC goes through an AC/DC converter and the DC goes through a power manager circuit that either directly is feeding the sensor, RF interface or the CPU, any residual energy is forwarded to the energy storage. Due to the often stochastic feed from the harvester, small chunks of energy come to the power manager which needs a clever algorithm to be able to distribute the energy properly. The power consumption is often a limiting factor and the power manager repeatedly needs to gather enough energy from the harvester to power the onboard RF interface, which is sending in intervals [23].

The MIDE EHE004 is the energy harvesting power manager used with the piezoelectric energy harvesters in this thesis. It has a full wave rectifier with charge management and DC conversion. The output can be chosen to the following settings: 1,8 V, 2,5 V, 3,3 V and 3,6 V, where 3,3 V is the choice in this thesis due to the input demand from the RF interface used. It also has the option of connecting auxiliary energy storage where enough power can be stored to start up the RF interface or act as a backup if there is a period where no ambient energy is present.

1.3.2 The intelligent sensor

An intelligent sensor interprets the collected data from the sensor by a microprocessor which makes calculations and analyses the data from given boundaries. If the analyzed result needs to be transmitted, the data is compressed and the information will be sent to a central unit. The sensor and the microprocessor have to be one physical unit to be called an intelligent sensor. A sensor where the only function is to detect and send an unprocessed signal to an external system, which then performs some action, is not considered intelligent. To make the intelligent sensor more effective, a network of sensors can be setup that works together is in a so called wireless sensor network (WSN) as mentioned in paragraph 1.1 [24], [25].

An intelligent sensor can be defined as:
   "A smart sensor provides various functions beyond those necessary to generate better decision making or better controlled quantity. The intelligence aspect is improved in a networked environment" [26].

Is an intelligent sensor smart and or intelligent? Or is it just a label we describe them with, since an intelligent sensor is monitoring something, all the time. By putting many sensors together, the decision pattern can mimic something we would call an intelligent pattern where the outcome is to perform a (for a human) simple task. In addition, more important where do we, humans, draw the line for tasks being performed based on decisions made, established on intelligent sensors input. It is nice and comfortable to hand over tedious monitoring tasks to intelligent sensor systems, but questions remain, if we cross that line, will intelligent sensor based systems have hiccups? Like not passing on vital information, not due to malfunction, but decisions based on input from the intelligent sensors, which might cause death [27]. We are not there yet, and answers about the future is not easy to predict. However, as long as we implement advanced intelligent wireless sensor systems based on a proper investigation, we hopefully will not find ourselves surrounded with systems deciding what is best for us and not the other way around.

An example where many sensors are used to perform a simple task is a robotic vacuum cleaner, shown schematically in Figure 1.4. In order to be able to conduct cleaning, the robot has to navigate in rooms with obstacles in the vicinity. Mechanical bumpers, in the front, can be used to detect when the robot touches a wall or an obstacle. Proximity sensors that utilize infrared or ultrasound can also be used for the same purpose. Under the robotic vacuum cleaner, you will need sensors to detect the absence of surface (cliff sensors), like when encountering a stair. For localization and mapping there are different options to choose from:

- Cameras
- Ultrasound sensors
- Laser rangefinder
- Wheel encoders

Then there is the task of cleaning, for which you need sensors that sense the bin level, battery level, brush being stuck and detecting dust on the floor [28], [29]. All sensors put together with the task to clean and charge itself, actually make the robotic vacuum cleaner an advanced autonomous intelligent sensor system.
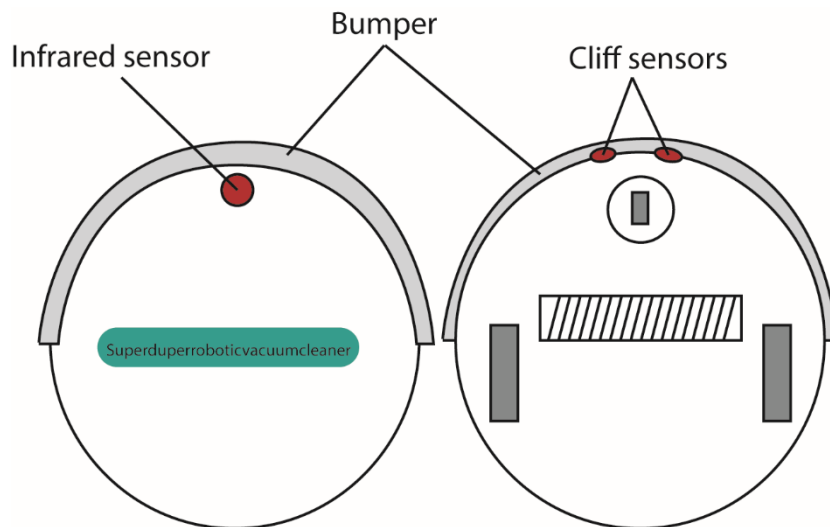
Figure 1.4, Schematic of a robotic vacuum cleaner with sensor positions, top (left) and bottom (right) view.

1.3.3   Energy storage

1.3.3.1   Batteries

Today batteries are the main energy source for IWS [30]. The advantages of batteries are their high energy density, as presented in the schematic Ragone plot [31] in Figure 1.5. The foremost drawback when using primary batteries is that they have to be replaced when depleted. If secondary batteries are used in conjunction with a harvester, the number of rechargeable cycles are still very limited (<1000) [17] and thus they too eventually have to be replaced. The increasing amount of

disposed batteries is also a major environmental concern, as recycling still is very low even though loads of research on recycling for the hazardous components in batteries are performed [32]–[37].

1.3.3.2 Supercapacitors

Supercapacitors, also named ultracapacitors have attracted attention because of their capability of fast power intake and release (Ragone plot in Figure 1.5), their long cycle life and that they are eco-friendly. Supercapacitors are used as backup power for computers, power booster for forklifts, and power source from brake energy recovery for brake systems in hybrid vehicles among many other applications [38]–[43]. Despite its lower energy density, the supercapacitor is a good choice compared to batteries due to its high number of recharge cycles (10^6). Therefore, over its lifetime, it reaches a higher accumulated energy density than batteries, as shown in Paper VI.
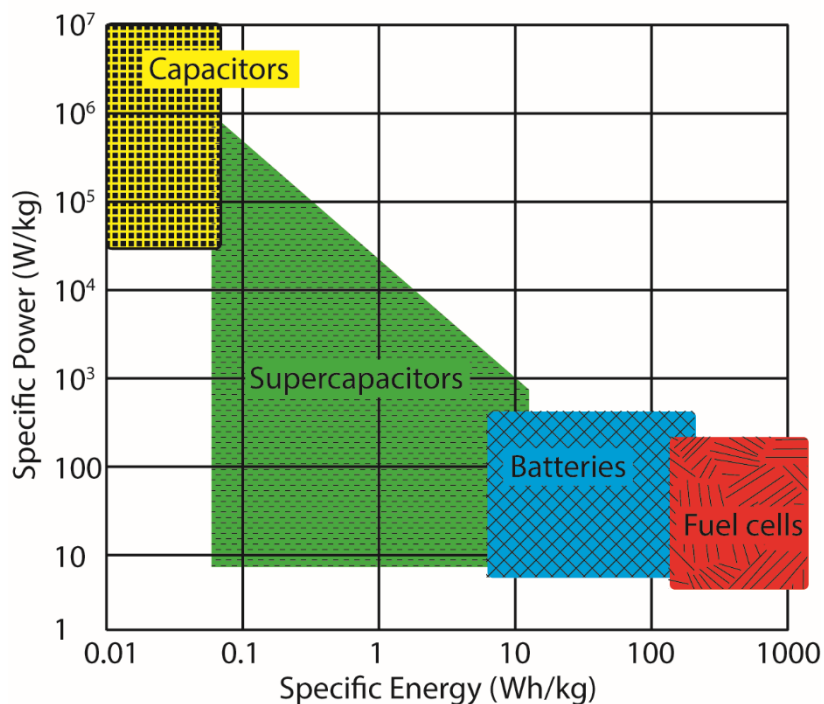
Figure 1.5, Schematic Ragone plot for energy storage and conversion devices. The indicated areas are rough guide lines between the different storage techniques. The Y-axis indicates how fast an energy storage can unload or load its power and the X-axis indicates how much energy it can store.

1.3.4 Energy harvesting

To gain greater strength than the human body could muster, or have energy for long tedious tasks, humanity had to scavenge energy from its surroundings and convert it into usable energy. Hence the first harvesters were born in the shape of the waterwheel and the windmill [44]. Humanity has since continued to harvest energy from ambient renewable sources and today primarily converts it to electric power by e g water turbines, wind turbines, photovoltaic cells and thermoelectric converters.
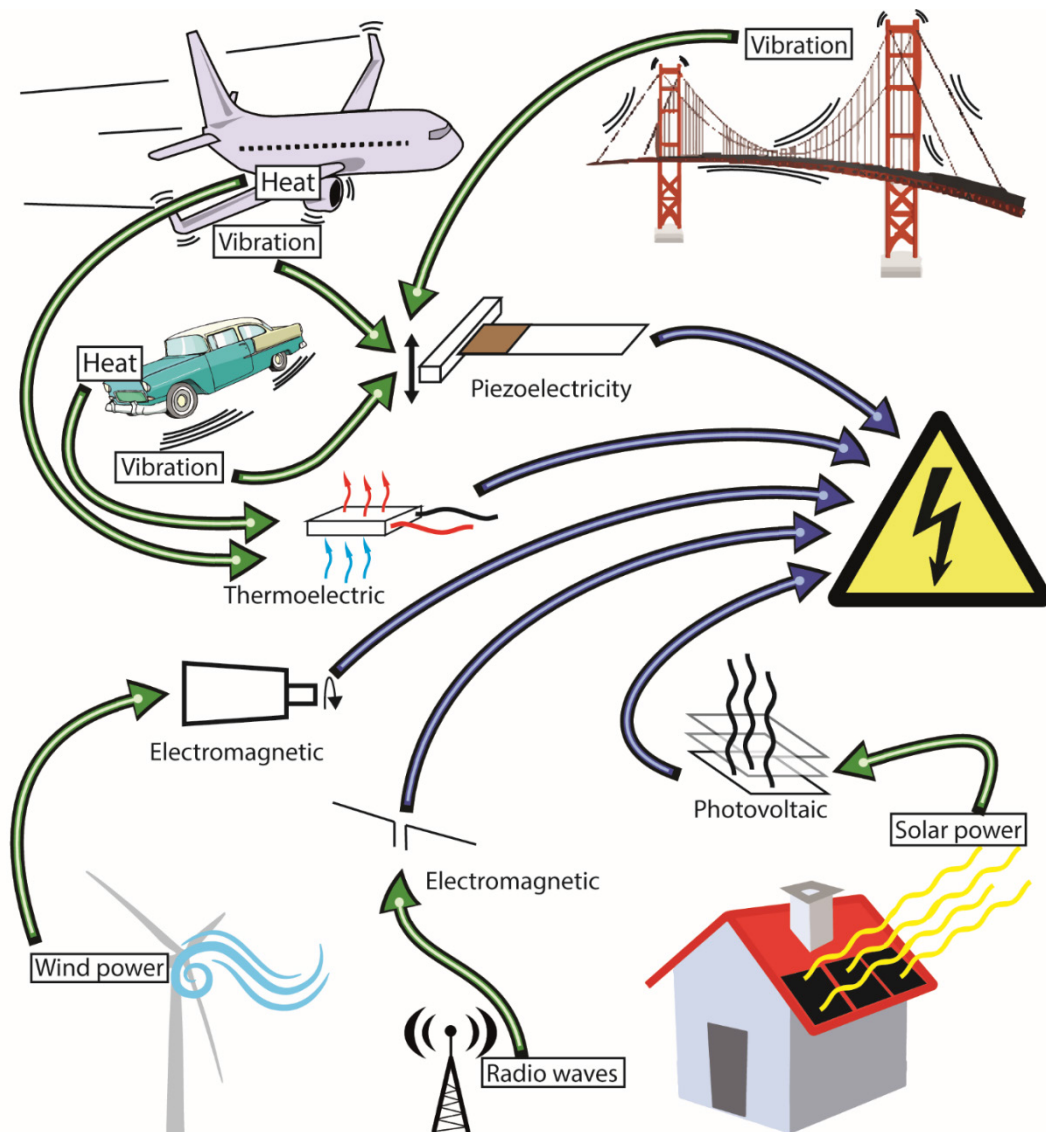
Figure 1.6, An overview of energy harvesting from different ambient energies with conversion to electricity.

Depending on the location of the AIWS system, different ambient energy sources can be utilized to power it (Figure 1.6). Small AIWS are used for applications such as:

- Environmental monitoring
- Surveillance
- Structural monitoring
- Interaction and control
- Medical remote sensing
- Military applications
- Aerospace

By applying powering through energy harvesting in such AIWS applications, benefits will arise in the terms of the AIWS becoming maintenance free. Then it can be placed in inaccessible sites where operability else would be impossible due to impractical cable length or that the AIWS is permanently built into a structure. Smart choices of energy harvesting and energy storage will increase the operability of the AIWS. By substituting batteries with energy harvesters, we will have a big cost saving by not having to replace batteries, eliminating also the need to handle their chemical disposal [32]–[37].

In a specific case, a gas turbine, two main ambient sources of energy are found: heat and vibrations. Thus, energy can be harvested by thermal harvesters and by kinetic piezoelectric harvesters. On a test site, the number of sensors is counted in hundreds and the cable length per sensor is hundreds of meters. Reducing the usage of cables on test sites will make the testing much easier and faster. In the future, reducing the amount of cables to sensors, on the gas turbine mounted to an airplane, will make the engine weigh less and therefore also use less fuel. To prolong operation time of the AIWS the main challenge today is to replace batteries with energy harvesters [45], [46].

2 PIEZOELECTRIC VIBRATION ENERGY HARVESTING

In this chapter, piezoelectricity is scrutinized. By its mechanism and how to harvest energy with mechanically coupled resonators, in the shape of a piezoelectric harvester are described. The development of new designs for piezoelectric harvesters to be used for gas turbine applications is presented. The impact of conjoining two cantilevers is covered, which utilizes extended stress distribution, and is presented on: a backfolded harvester, a self-tuning harvester and a micro harvester.

2.1 PIEZOELECTRICITY

In 1880 Jacques and Pierre Curie demonstrated the piezoelectric phenomena [47] based on their knowledge in pyroelectricity and of the basic crystal structures to forecast the behavior of crystals with piezoelectric properties [48]. Piezoelectricity is an electric charge that is accumulated in crystals [49] , some ceramics [50], can be found in DNA [51], [52] and specific proteins [53], when a mechanical stress is applied. The first application to utilize piezoelectricity was a sonar device developed by Paul Langevin 1917 in France [49]. It was used to detect submarines and was made of a transducer, which was composed of thin quartz crystals, packaged in glue between two steel plates. It was connected to a hydrophone, which detected the echo that was returning from the submarine. By measuring the time until the echo was heard, the distance to the submarine could be calculated. Today a popular application for piezoelectric ultrasound transducers is to mount them on the rear of many cars and help the driver to conclude if any object is directly behind the car and therefore not visible to the driver [54].
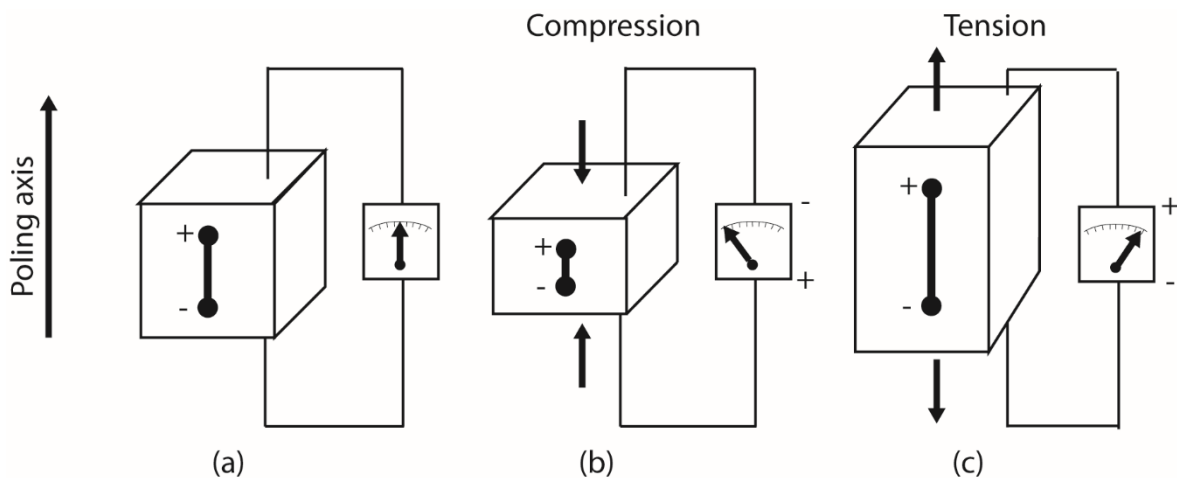

Figure 2.1 Overview of direct piezoelectric effect; (a) Piezoelectric material after poling under no impact of strain, (b) Energy generation under compression, where the voltage has the same polarity as poling voltage (c) Energy generation under tension, where the voltage has polarity opposite of poling voltage.

2.2 MECHANISM OF PIEZOELECTRIC MATERIALS

Piezoelectric effects are closely related to the existence of electric dipole moments in solid materials [55], [56]. The dipole polarization is calculated for crystals by adding the dipole moments per volume of the crystallographic cell [57], [58]. Each dipole is a vector and the dipole density P is a vector field. Dipoles near each other can be aligned in regions called Weiss domains. These domains are usually oriented in random order but can be aligned by using a process called poling. Poling is a process where a strong electric field is applied across the material, usually at elevated temperatures [59], [60].

A key importance for the piezoelectric effect is the change of polarization, P, when an external mechanical stress is applied and cause a re-orientation of molecular dipole moments, Figure 2.1. Piezoelectricity will be produced depending on the variation of the polarization strength, the direction or both. It depends on:

- The orientation of P within the crystal.
- The crystal symmetry.
- The applied mechanical stress.

Piezoelectric materials also show the opposite effect, called converse piezoelectric effect, where the application of an electrical field forms mechanical deformation in the crystal. The combined effect of material behavior gives the piezoelectricity (2.1), (2.2). First effect:

$$D_i = \varepsilon_{ij} E_j \qquad (2.1)$$

where D is the electric charge density displacement, ε is permittivity and E is the strength of the electric field. Second effect is Hooke's law:

$$S_{ij} = s_{ijkl} T_{kl} \qquad (2.2)$$

where S is strain, s is compliance and T is stress.

These two material effects are combined in coupled equations where the strain-charge in matrix form is:

$$\{S\} = [s]\{T\} + [d^t]\{E\} \qquad (2.3)$$
$$\{D\} = [d]\{T\} + [\varepsilon]\{E\} \qquad (2.4)$$

where $[d^t]$ is the matrix for the converse piezoelectric effect and $[d]$ is the matrix for the direct piezoelectric effect. Equation 2.3 represents the connection for the converse piezoelectric effect and 2.4 the direct piezoelectric effect [61].

2.3 PIEZOELECTRIC CANTILEVER HARVESTING: DEVELOPMENT AND CHALLENGES

To utilize the direct piezoelectric effect, piezoelectric crystals may be packaged in thin films for attachment on a cantilever at the clamped end, where the stress/strain is highest, as presented schematically in Figure 2.2 . By applying vibration to these cantilevers, an AC voltage is obtained. The energy produced is usually in μ-mW range and is too small for large electrical applications

depending on power demand but yield enough power for a small electronic system like an intelligent wireless sensor [62]. It is hard to directly compare piezoelectric vibration harvesters, since they employ different techniques and since the variation in sizes. Between a couple of μm for MEMS fabricated harvesters up to meter size for macro harvesters, make them behave radically differently [63]. A defined standard figure of merit (FOM) would be beneficial. However, none of the several FOMs that have been suggested have resulted in any standardization [64].
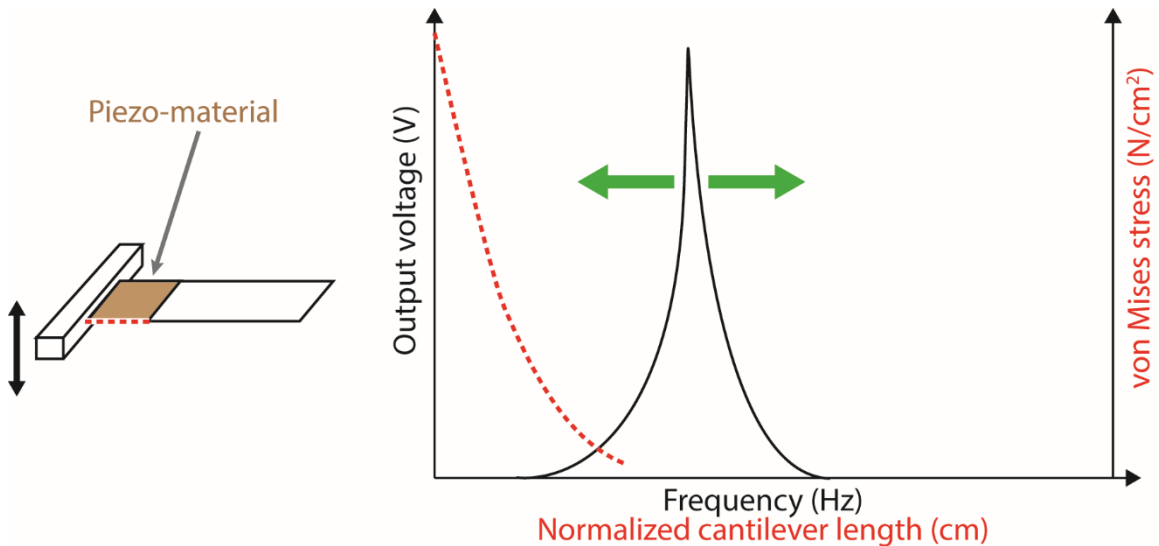
Figure 2.2 A SDOF schematic piezoelectric cantilever with piezoelectric material attached at the fixed end. In the graph, a high-power output peak with the typical narrow bandwidth for the lowest eigenfrequency is presented. The green arrows present the output curve's change if the bandwidth increases. The dotted red line is a schematic representation of stress along the cantilever.

The main problem for piezoelectric single degree of freedom (SDOF) cantilever harvesters is ending up with the main power carrying frequency residing outside the optimized narrow frequency range of the harvester. The output power drops dramatically outside the range of the lowest eigenfrequency resonance peak of the cantilever, presented generally in Figure 2.1. The placement the of piezo material is at the clamped end, where the stress is highest on the cantilever; the stress decreases rapidly towards the free end of the cantilever and only a small part of the cantilever is actually used for energy harvesting as presented schematically in Figure 2.2. Over the years several methods have been suggested on how to broaden the bandwidth of piezoelectric cantilever harvesters, without significantly sacrificing the output power [65]. These different approaches can be classified into:

- Multimodal harvesting [66]–[68].
- Self-tuning [69]–[71].
- Resonance tuning [72]–[74].
- Nonlinear technique [75]–[77].

In this thesis, multimodal and self-tuning harvesting is covered. Improved approaches have been covered in the literature on multimodal energy harvesting, where some have made comparable systems using an array of cantilevers combining different lengths and weights to cover a broader bandwidth. By tuning each one for a different frequency as presented in the schematic Figure 2.3 [78]–[80] a broader bandwidth is achieved. Using an array of cantilevers where only one cantilever will be able to harvest effectively, each at the time, the design will become bulky in size if the array is to be able to harvest over an extensive bandwidth.
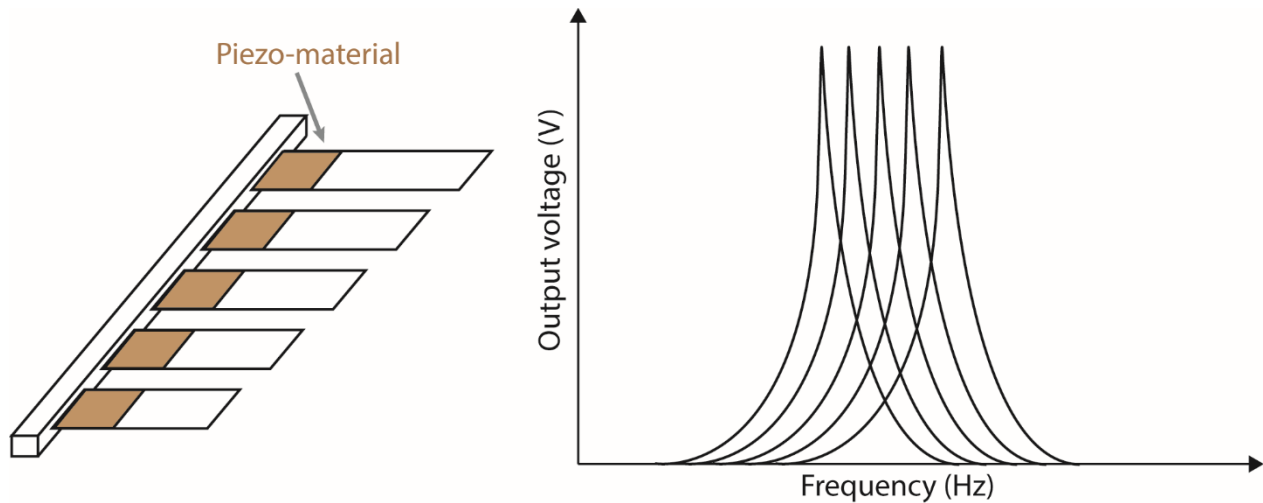
Figure 2.3 Schematics of an array of piezoelectric cantilevers, able to yield a power output over a broader bandwidth, compared to a single cantilever. Only one cantilever at the time is able to effectively target the applied frequency, hence to target an extensive bandwidth the design quickly becomes immense.

An example of multiresonance energy harvester developed by Qi et al. (2010) [81], has arrays of cantilevers attached to a single beam in the middle. Even though the design is cunning, the bulk and weight of the harvester limits its power density and therefore its usability.

An alternative to the array structure is the multiple degrees of freedom (MDOF) energy harvester that was developed by using a single beam [82]. One case of MDOF is the two degrees of freedom (2DOF) that has two masses on a cantilever as presented in Figure 2.4. By this design two modes are obtained, but the two peaks are still too far away from each other to be considered a broadband harvester [83]. An enhancement of the 2DOF design was made using a dynamic magnifier; this magnified the power output from the piezoelectric outer beam in the two-beam system, where the inner beam acts as a magnifier for the outer beam [84]. Most designs for multimodal energy harvesters have the resonance frequencies separated from each other and usually the second peak has lower power output than the first one as presented schematically in Figure 2.4. The frequency spacing between the peaks is also a problem and you should have the secondary peak closer to the primary peak so that the range in between the peaks can be used for energy harvesting.

Figure 2.4, A schematic 2DOF cantilever with 2 masses. The graph prsents the power output for the two first eigenfrequencies where the second yields less power (shown by the orange trendline). The green arrows indicate that the secondary peak has to be closer to the primary peak to be able to get higher power output between the peaks, thus a more broadband harvester.

H Wu et al. (2012) [85] proposed a 2DOF piezoelectric energy harvester with a cut-out design where the two modes are nea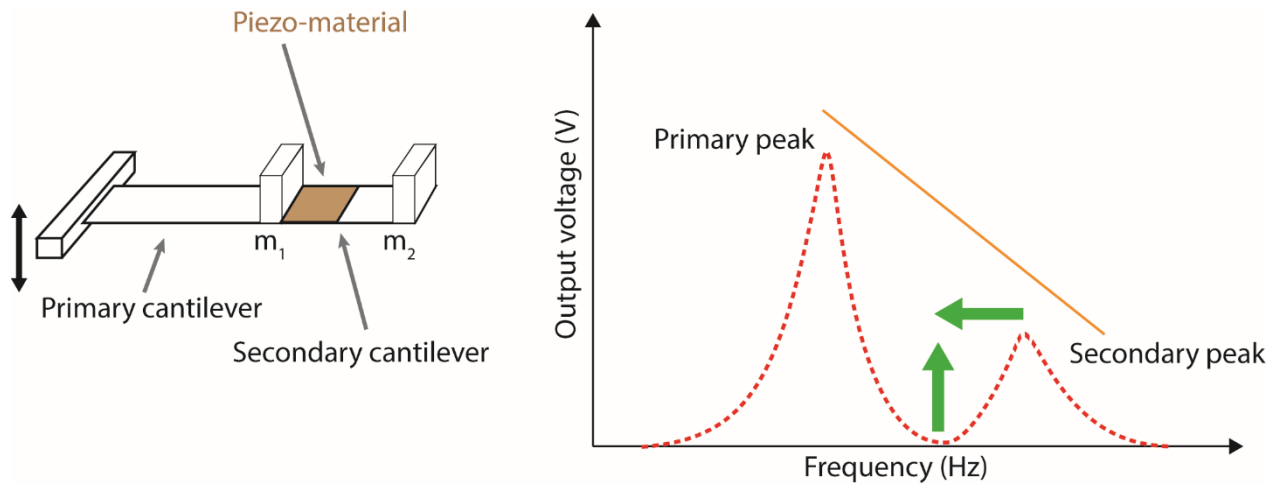r each other and the second mode also has a good energy conversion. This design looks very promising considering the energy density. However, the design only utilizes one cantilever with piezoelectric material at the attached coupled end and the design is also bulky.

Challenges for vibration energy harvesting using piezoelectric cantilevers:

- Only a small part of the cantilever is used for energy harvesting.
- The harvesting bandwidth is narrow.
- Solutions to broaden the bandwidth tend to increase the size of the harvester.
- Solutions to broaden the bandwidth tend to decrease the power output.

This thesis attend to and make proposals toward solutions to these challenges.

2.4 ACHIEVING BANDWIDTH AND POWER ENHANCEMENT

To be able to utilize the benefits of an IWS it has to be practical in size to fit in small places like on an engine or a gas turbine. All electrical components in the IWS are small and naturally the space available in the neighborhood of a gas turbine is limited, therefore the harvester has size constraints. In order to meet those constraints using conventional commercial piezoelectric cantilevers, new harvester designs are needed. Such as structures which could utilize more of the cantilever bulk, not only the fixed end where it is attached, to harvest energy. This would make the harvester able to decrease in size and might have a maintained or even increased power output.

A new structure based on 2DOF principles was presented in Paper I. Previously, cantilever harvesters have utilized a primary cantilever to enhance a secondary one (Figure 2.4). In Paper I, the primary cantilever is piezoelectric as well as the secondary cantilever (Figure 2.5). Instead of

placing the two cantilevers in the same plane, the secondary cantilever is backfolded over the primary cantilever as presented schematically in Figure 2.5. By this design, the projected area becomes smaller compared to a 2DOF harvester in one plane. Even though the design becomes somewhat higher, it requires less operational volume than a 2DOF harvester in one plane due to shorter cantilevers and less displacement compared to a 2DOF with longer cantilevers in total. The piezoelectric cantilevers used in the design are off the shelf (OTS) and manufactured by MIDE. The choice of OTS beams was based on their availability, small enough size and that they would be used in a gas turbine demonstrator, where components are demanding robustness and that the demonstrator can easily be reassembled.

The design was simulated in finite element analysis, (using the finite element analysis COMSOL software). Measurements on the MIDE cantilever was compared with simulation data to have a reliable model to be able to simulate the behavior of the backfolded design. When the backfolded design was simulated, the first result was that the output voltage was different from a general 2DOF system. The primary output peak had the same behavior, but the secondary peak had a maintained voltage output comparable to the primary peak, presented schematically in Figure 2.5. To get a better benchmark comparison, the design in Paper I was compared with two tuned single cantilevers, since the general 2DOF only have one patch of piezo material, while the backfolded design has two. One single cantilever was tuned to the primary peak and one to the secondary peak. The two single cantilevers where added together for a total simulated open voltage output and compared with the backfolded, as presented in Paper I. The simulated backfolded harvester outperformed the two single tuned cantilevers.
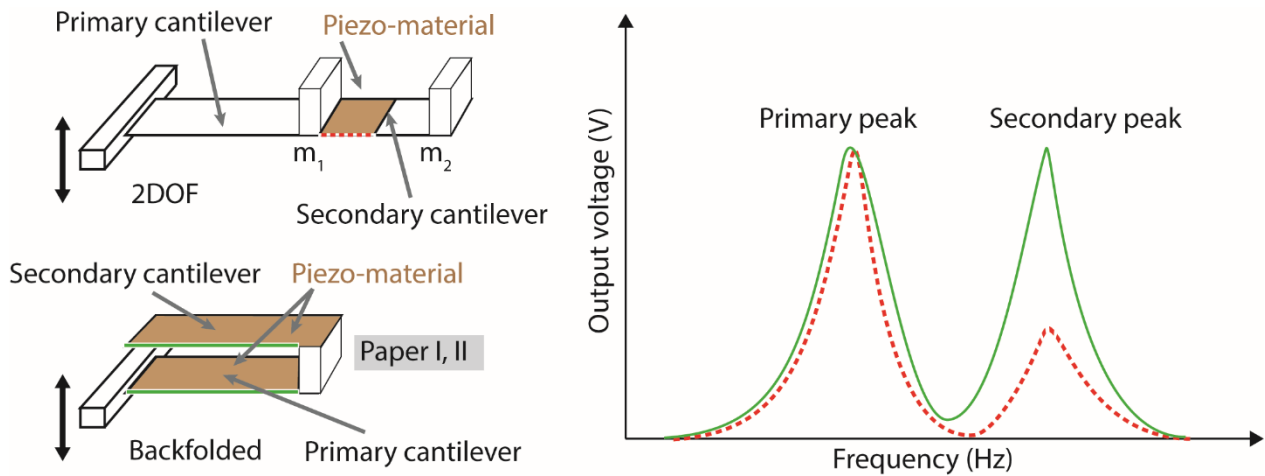

Figure 2.5, A schematic 2DOF harvester compared with the schematic backfolded design. In the graph the green line represents the general output voltage from the backfolded design. The secondary peak has a maintained voltage output comparable with the primary peak.
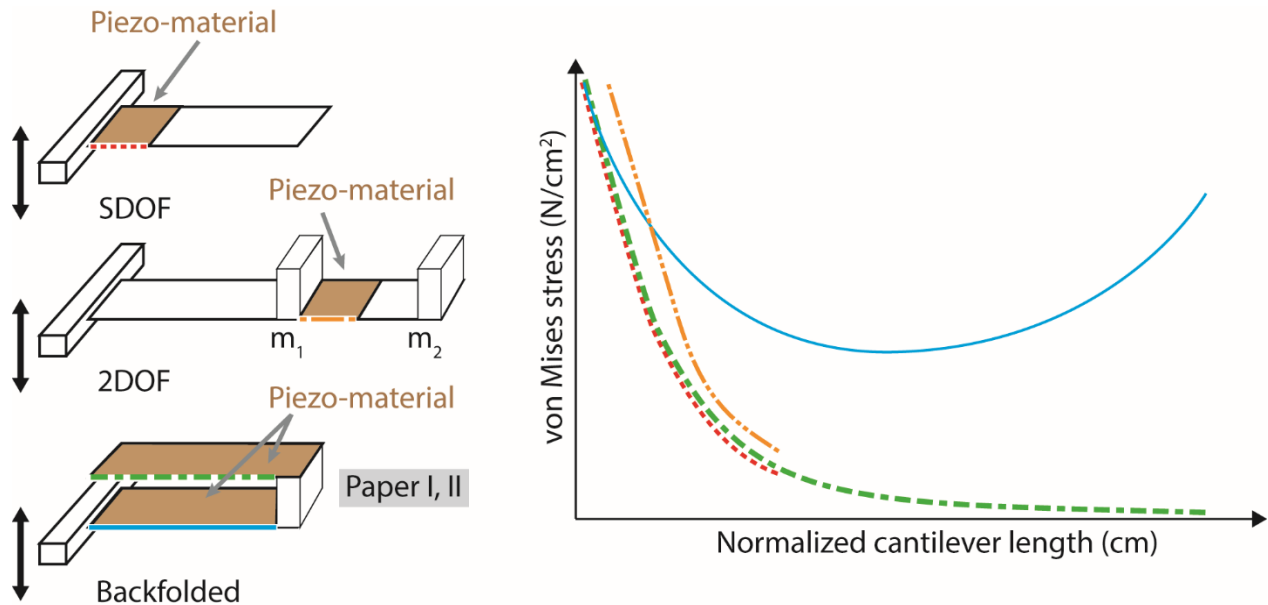
Figure 2.6 Schematics of three designs; SDOF, 2DOF and backfolded. In the graph general stress are presented where the difference between the curves are the blue line representing the bottom cantilever where the stress is distributed over the whole cantilever area compared to the other stress curves which are decreasing rapidly.

In order to understand this effect, stress data from simulations were compared for the single cantilever and the backfolded harvester. In Figure 2.6 the different plots of the general stress, depending on design, is presented schematically. For the single cantilever, the stress is highest at the attached end (dotted red line). For the enhanced harvester based on 2DOF it shows the same behavior (dot-dot-line orange line), but it is higher compared to the single cantilever. For the backfolded design, the top cantilever shows the same behavior as for single and 2DOF (green line). The big difference is when we examine the bottom cantilever of the backfolded design, there we can see that the stress curve is extended and distributed over the whole cantilever (blue line). The elevated stress explains why the backfolded design has a higher output. As presented in Paper I, the measured output correlated with the simulated.

Even though the power output was maintained for the secondary peak on the backfolded design, the primary and secondary peaks have a separation, ΔHz (from peak to peak), that is too large and needs to be decreased to utilize a broader bandwidth effect. When the two peaks have a small ΔHz the valley will effectively rise between the peaks and yield an increased power output which leads to a broader bandwidth presented schematically in Figure 2.7 indicated by the blue arrow. The backfolded design was extensively measured for in total 144 different combinations to provide data for a simplified numerical model used in Paper II. From the data it became clear that for the three different clamping positions of the bottom cantilever (presented in Paper II) three distinct groups of ΔHz between the two peaks were identified. Within these three groups the two masses (m_1 and m_2 in Figure 2.7) were altered. For all design combinations the ΔHz was still too high for the peaks

to be bridged (Figure 2.7). In Paper II, the numerical model predicts that the peaks will have a lowest ΔHz if the top cantilever is approximately 20% shorter than the bottom cantilever where $m_1 = m_2$. Which was confirmed by measurements. However the configuration yielding the closest ΔHz, did not yield the best output from a harvesting point of view. Clarifying the difficulties with conjoined cantilevers as energy harvesters.
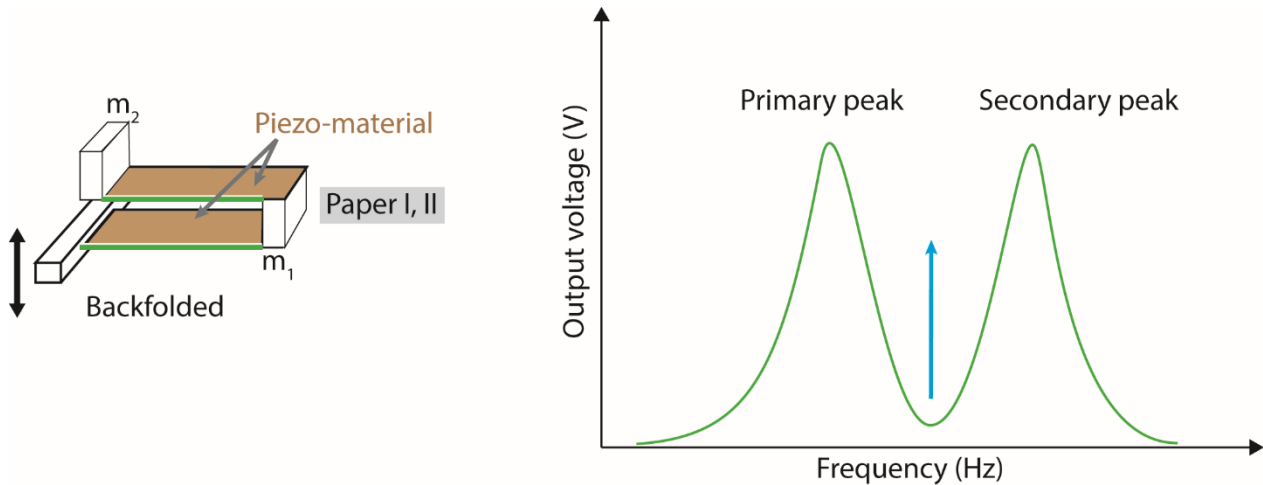
Figure 2.7 By shortening the length of the top cantilever, the primary and secondary peaks get a decreased ΔHz and the output voltage in between them gets higher (indicated by the blue arrow). Hence the backfolded harvester gains a broader bandwidth.

2.5 INCREASED BANDWIDTH BY NON LINEAR SELF-TUNING HARVESTING

To achieve broad bandwidth the concept of self-tuning can be applied. A self-tuning piezoelectric harvester has the ability to adjust its eigenfrequencies to match the applied ambient frequency. When the eigenfrequency shifts for the harvester, the high Q-value is maintained. This means that the power output remains significant over a broader bandwidth, where the structural eigenfrequencies adjusts to the applied ambient frequency. The change in eigenfrequency can be performed during ongoing harvesting or in between when no harvesting is done. Preferably, the eigenfrequency is automatically adjusted during harvesting. This can be done using electric adjustment systems [86]–[88] or by using mechanical solutions [10], [11], [30]–[32]. Mechanical solutions are slower to adjust to the eigenfrequency compared to electrical ones, but they have the positive trait of no power consumption, which tends to be a problem for electrical self-tuning solutions [92]. The choice to use resonance tuning by automated mechanical self-tuning is preferable if the main frequency mode is changing slowly over time, like in an engine. A harvester that has self-tuning uses input from the ambient vibration to adjust its frequency. It can for example be a rotational acceleration force [69] or a bistable system that can change between two stable states [70]. A mechanical tuning effect was demonstrated by Miller et al. [93], presenting that for a given excitation at a certain frequency, a sliding proof mass will move on a beam until it reaches a position where the mode of vibration has a resonance behavior. This was presented experimentally

for a double clamped beam [93], where the proof mass could alter its position (marked as sliding mass in Figure 2.8), as the driving frequency changes, in order to maintain resonance.
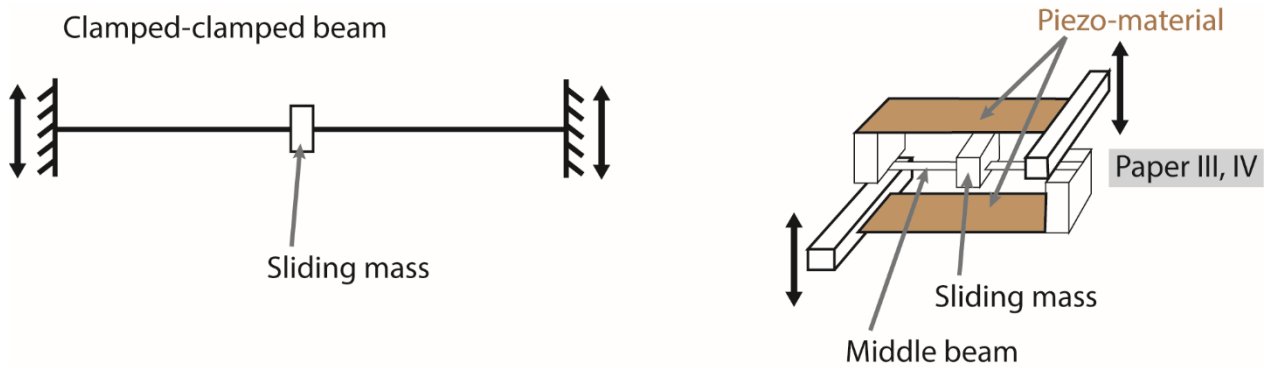
Figure 2.8 To the left the clamped-clamped beam with a sliding weight, to the right the self-tuning harvester based on the backfolded design and the sliding mass phenomenon.
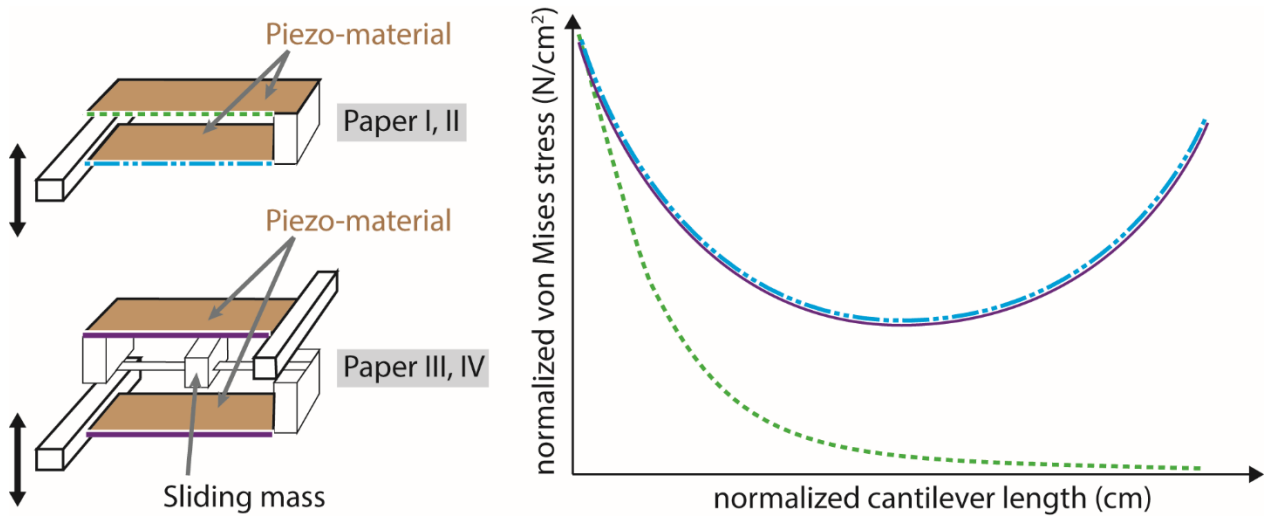
Figure 2.9 To the left top is the backfolded design presented in Paper I and II, below is the self-tuning harvester which utilize the extended stress distribution in Paper III and IV. To the right a schematic graph shows the stress curvature for the two harvester's individual cantilevers.

In order to utilize the demonstrated sliding mass phenomenon as a mechanical self-tuning effect, the backfolded design from Paper I and II was put together with a beam having a sliding mass, as presented in Figure 2.8. By using the backfolded design, the first trait was that the harvester size could be small. The second trait was that the extended stress distribution could be maintained for both piezoelectric cantilevers. In Figure 2.9 the backfolded design (Paper I and II) stress curvature for the top and bottom cantilever is compared schematic with the stress curvature for the self-tuning harvester (Paper III and IV). As presented, the two piezoelectric cantilevers stress curves (purple

line) from the self-tuning harvester behaves similarly like the bottom cantilever from the backfolded design (blue line).

The self-tuning design was presented at PowerMEMS 2015 [94], where conducted COMSOL simulations predicted that the eigenfrequency was shifting, depending on where the mass was positioned on the middle beam. This is somewhat similar to an array of cantilevers, but much smaller in size as presented schematically in Figure 2.10. Experiments verified that the bandwidth became broader when the mass was sliding compared to being fixed on the middle beam. Comparison between a short and a long middle beam showed that the power output was higher for a harvester setup where the middle beam was longer as presented in Figure 2.11. Experiments also showed that there was no difference in bandwidth between the short and long middle beam as presented in Figure 2.10.

The two measurements cases with short and long middle beam were referred to as M1 and M2 with data tabulated in Table 2.1. The difference in length between M1 and M2 indicates that the middle beam has different eigenfrequencies. A rough estimation of the clamped-clamped middle beam eigenfrequency is presented in Table 2.1. Since the output was increased when the middle beam had a lower eigenfrequency, three thicknesses (Test 1 – 3, Table 2.1) for the middle beam were tuned to match the harvester eigenfrequency. Experiments showed that the 0.35 mm middle beam gave the highest output (Table 2.1). The quite narrow bandwidth of 12 Hz (compared to Miller et al [93] with wide mechanical bandwidth of 95 Hz) was maintained for all three tests.

	Thickness (mm)	Width (mm)	Length (mm)	Calculated eigenfrequency (Hz)	3dB Bandwidth (Hz)	Measured maximum voltage output (V)
M1	1	3	16	2974	12	3.2
M2	1	3	27.5	1006	12	11.7
Test 1	0.7	3	27.5	760	12	14
Test 2	0.35	3	27.5	380	12	22
Test 3	0.175	3	27.5	190	12	12

Table 2.1 Tabulated structure data for the middle beam.

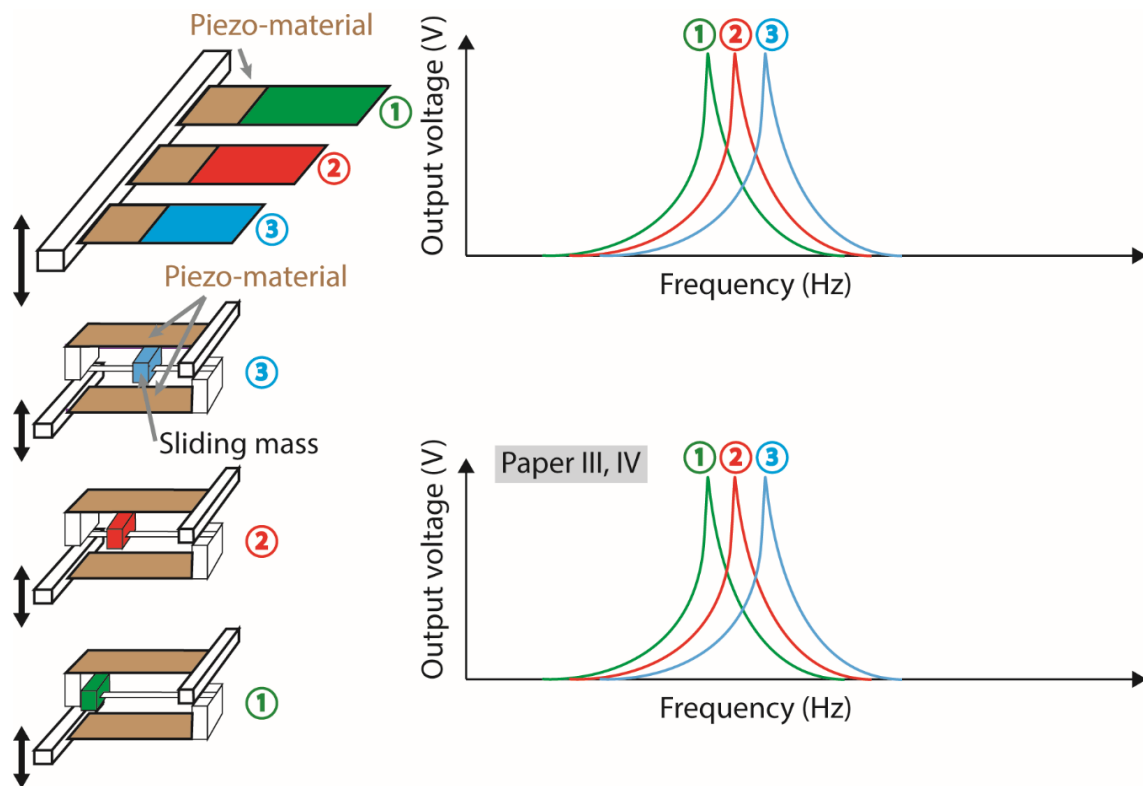*Figure 2.10 Schematically an array of cantilevers with different eigenfrequencies compared with a selftuning harvester is presented, where the sliding mass is marked with corresponding color and number for matching each cantilever on the array harvester.*
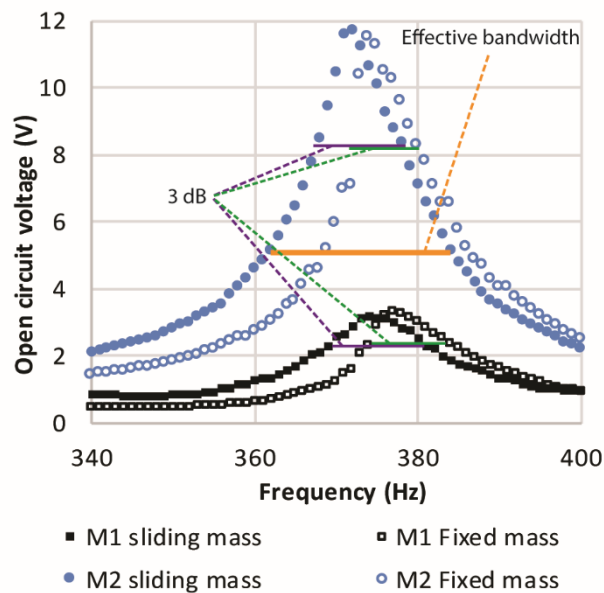

Figure 2.11 Open circuit voltage comparison between M1 and M2 with fixed and sliding mass for both. The output in M2 is 11.7 V and has a 3dB bandwidth of 12 Hz.

Since length and height modifications on the middle beam did not have any impact on the bandwidth, a numerical investigation on what modifications on the harvester that would have an impact on the bandwidth was started. The measurements from M1 and M2 were the foundation towards a numerical model, presented in Paper III. The model predicted that the highest impact regarding bandwidth was to introduce an asymmetry by different lengths for the piezoelectric cantilevers. The numerical model handled the beam system from a mechanical view and the predicted mechanical bandwidth was 60 Hz. The numerical model also indicated that the sliding mass was moving along the middle beam according to where the zero-slope was positioned (x) as presented in the schematic Figure 2.12 and a is the distance between the position of the sliding mass and the zero slope while η is the position of the mass on the middle beam. The zero-slope position itself is dependent on the applied frequency.
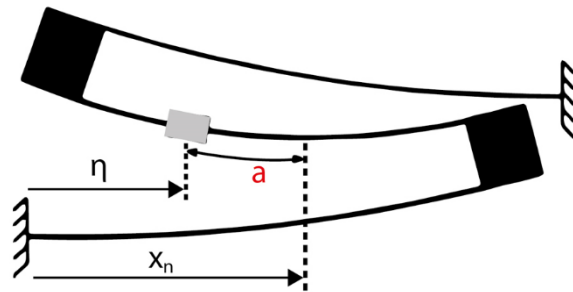
Figure 2.12 For the first mode, the outer masses move in the same direction and the position of the sliding mass (η) can be related to the position (x_n) with zero slope of the middle beam where the distance a $_{=|x_n-\eta|}$

The numerical model calculated the eigenfrequency depending on where the mass was located on the middle beam. For these eigenfrequencies it is interesting to see the mode shape of the middle beam. In Paper IV the mode shapes for one case L3 with mass configuration C1-C4 (Table 2.2) were presented and a brief discussion about the correlation was presented. Aiming at a deeper understanding of the phenomenon, the model prediction for the sliding mass position and its behavior, configuration L3/C1 will be examined more closely (on cross section L3/C1 marked in green in Table 2.2). For L3/C1 the sliding mass shifts from a position to the left of the middle beam to a position near the right side of the middle beam, during the frequency sweep as presented in Figure 2.13. Looking at the output curve the self-tuning effect is visible between 194 Hz – 201 Hz. Above 201 Hz the sliding mass has a stable position up to 213 Hz and in this range, we have a clear power peak for the harvester system. From the numerical model presented in Figure 2.14, the calculated mode curves for L3/C1 describes where the zero slope is positioned for a certain position of the sliding mass at an eigenfrequency. In the numerical model the fixed mass position is in some cases not the position where the sliding mass will stay, if the zero slope is located at another position. In the numerical model when the sliding mass is located at $\eta = 0$ on the middle beam, the zero-slope position is at $x_n = 1$ on the middle beam (Table 2.3 and Figure 2.13), where η and x start at 0 on the left side of the middle beam (Figure 2.12 and 2.14). This indicates that the mass wants to slide towards the right side (x = 1) as presented in table 2.3. The sliding mass is placed in four different positions on the middle beam, yielding four eigenfrequencies and three different zero slope positions (η), where η corresponds to the measured values x_m as presented in Figure 2.13.

Comparing the zero slope η with x_m (sliding mass position during measurement) in Figure 2.13 we can see that both have similar position behavior. The change in position is from 0 on the middle beam towards 1 and then back to 0 again. The numerical model has slightly lower eigenfrequencies for the sliding mass position compared with the measurement but gives a decent correlation to measurement, considering that the numerical model is a simple beam, point mass construction. Both the utilization of a self-tuning mechanism and the ability to predict its behavior are a key to achieving a broader bandwidth. I believe that self-tuning in combination with conjoined asymmetric cantilevers is a viable challenger to harvesters used today.

Measurements configurations	C1 No added mass	C2 One added mass on bottom cantilever (m)	C3 Two added masses on bottom cantilever (2m)	C4 One added mass on top cantilever (m)
L1 top/bottom	18 / 18	18 / 18 (m)	18 / 18 (2m)	18 (m) / 18
L2 top/bottom	20 / 16	20 / 16 (m)	20 / 16 (2m)	20 (m) / 16
L3 top/bottom	22 / 14	22 / 14 (m)	22 / 14 (2m)	22 (m) / 14
L4 top/bottom	24 / 12	24 / 12 (m)	24 / 12 (2m)	24 (m) / 12

Table 2.2 Mapped measured configurations for the self-tuning harvester. The marked green configuration L3/C1 with top piezoelectric cantilever 22 mm and bottom piezoelectric cantilever 14 mm is examined.

	Numerical model sliding mass position	Zero-slope position	Measured sliding mass position close to numerical eigenfrequency	Numerical model eigenfrequency
———	$\eta = 0$	$x_n = 1$	$x_m = 0$	f = 179.5 Hz
....	$\eta = 0.5$	$x_n = 1$	$x_m = 0$ (50 – 194 Hz)	f = 192.8 Hz
— .— .	$\eta = 0.8$	$x_n = 0.55$	$x_m = 0.5$ (201 Hz)	f = 202.5 Hz
- - - - -	$\eta = 1$	$x_n = 0.1$	$x_m = 0.3$ (213 Hz)	f = 205.5 Hz

Table 2.3 Presenting numerical model; eigenfrequency, mass position (η), zero slope position (x_n), measured sliding mass position (x_m) and eigenfrequencies
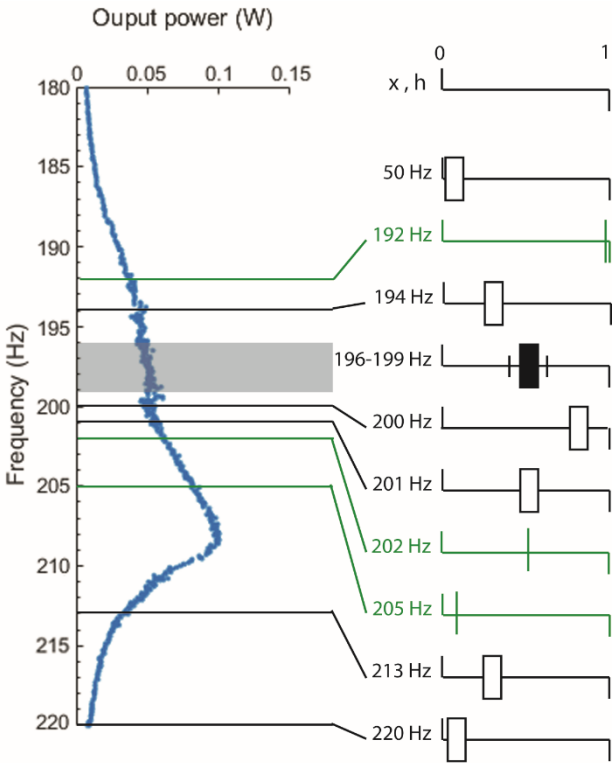
Figure 2.13 Presenting the output power for the configuration L3/C1, with marked sliding mass positions (white rectangles) and the black rectangle has an intermittent sliding behavior. The zero-slope position (green) from the numerical model is also marked.
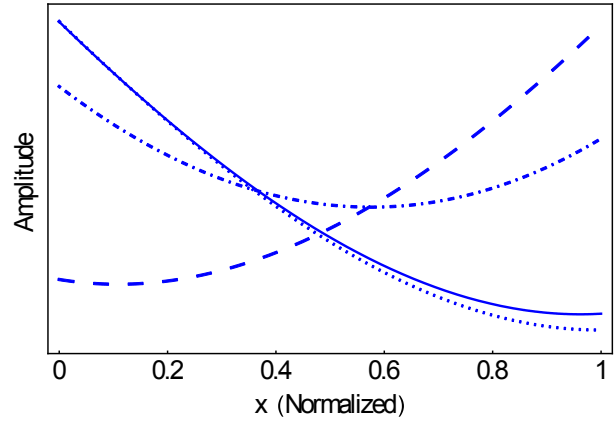
Figure 2.14 Presenting the numerical mode curves with different positions of the zero slope (x) depending on the mass position (η) on the middle beam

2.6 CONJOINED CANTILEVER MICRO HARVESTER

Circuits are decreasing in size and new ways of implementing intelligent sensors are ascending in the field of Internet of Things (IoT) [95]. Even though the gadgets are smaller, the problem with batteries that needs to be recharged or replaced remains. Harvesting energy for shrinking gadgets requires harvesters that also have to decrease in size. A micro energy harvester needs to be able to utilize all possible available area to be able to convert as much energy as conceivable. Different design approaches have been made but the most common MEMS design is to use a single cantilever. The reported frequency span is between 243 – 2300 Hz and the power output is between 0,471 – 2,7 µW [96]–[99]. Other designs used is a bent cantilever [100], circular spring [101], multiple cantilevers [102] and rectangular spring [103], where the multiple spring report the highest power output of 66,75 µW.
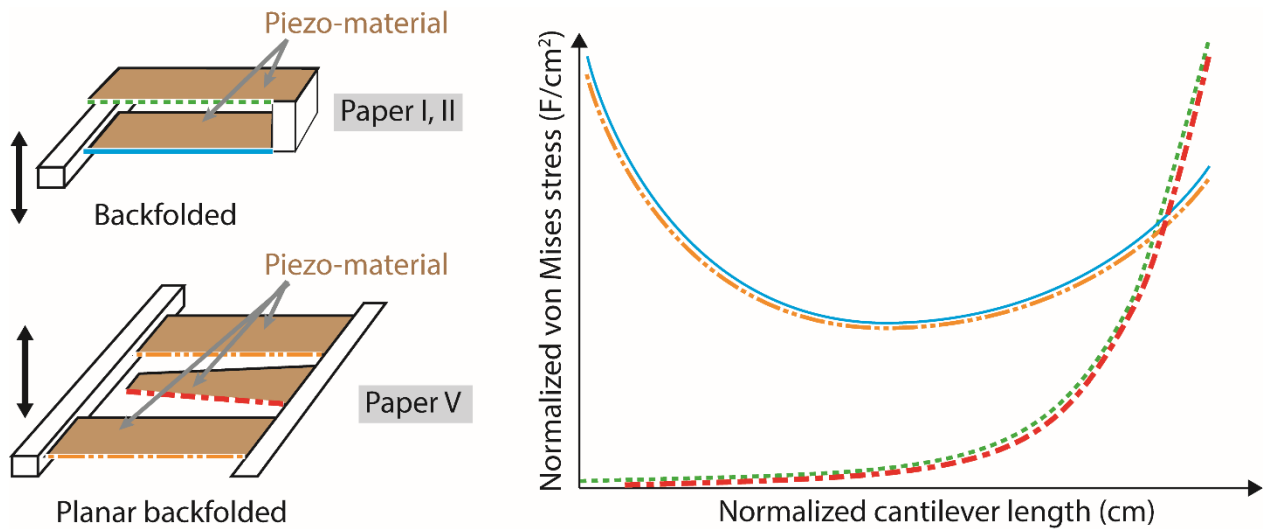
Figure 2.15 Presenting a planar backfolded design based on the top/bottom backfolded design. The planar design utilizes the extended stress distribution on the outer cantilevers and has a trapezoidal shape on the backfolded middle beam.

In the macro case (described earlier in chapter 2), it is of utmost importance to utilize as high amount of the available area as possible of the harvester. Due to fabrication issues a backfolded two layer design like in Paper I and II is hard to achieve. A similar concept but confined in one plane, is obtained by conjoining three cantilevers. In parallel with the backfolded design (stacked on top of each other) tests were made on a backfolded planar design. A planar design is desirable for micro production. As presented schematically in Figure 2.15 the planar backfolded harvester has two outer cantilevers and, in the middle, there is a backfolded piezoelectric cantilever. This design is possible to fabricate in micro size. To achieve a higher power output for the middle cantilever it uses a trapezoidal shape, which also yields a broader bandwidth [104], [105].

The design presented in Paper V looks promising for a micro harvester. Due to fabrication processing challenges, only a mechanical characterization of the harvester could be conducted (Figure 2.16). The primary peak was as predicted by simulations (Paper V), the secondary peak was a bit higher due to over etching of the backfolded middle beam mass. Despite the fabrication problem faced, I believe that conjoined cantilever harvesters are a good way to utilize as much available area as possible and show us a path towards upcoming more power efficient micro harvesters.

Figure 2.16 Measured mechanical characterization of the micro backfolded harvester.

3 SUPERCAPACITOR AS ENERGY STORAGE

In this chapter the supercapacitors are described by background theory and the specifications on electrode materials for supercapacitors used in IWS system. Electrochemical characterization by cyclic voltammetry and galvanostatic charge discharge is described and results of the electrode materials CNF and CNT, CVD grown, on CNF are presented.

3.1 BACKGROUND AND THEORY

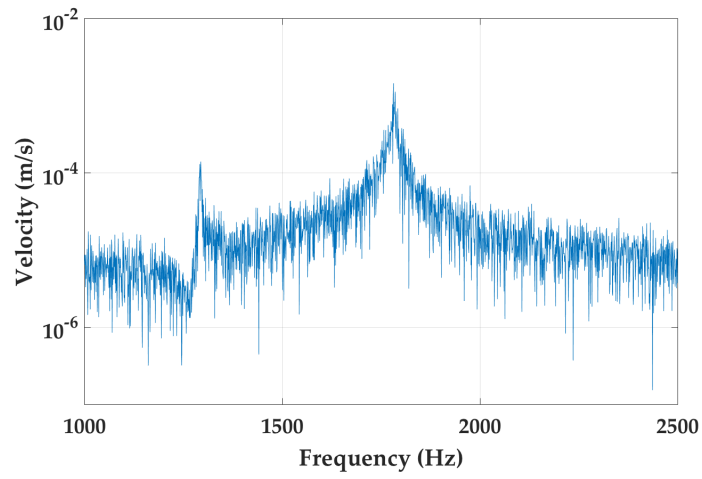A supercapacitor is an electrochemical capacitor with a very high capacitance. Supercapacitors, sometimes called ultracapacitors or electric double-layer capacitors (EDLC), do not have a conventional solid dielectric. Instead they use an electrolyte. In 1957, a patent filed by General Electric [106] explained the manufacturing of a device that used porous carbon electrodes with sulfuric acid between the electrodes [107]. After further development supercapacitors have been used since the mid-seventies as energy storage for backup computer memories [108]. Furthermore, supercapacitors have become useful for wireless communications and are used as power devices for different applications like recovering brake energy to improve energy efficiency in a hybrid battery/diesel system [40]. The energy density of a supercapacitor depends on the capacitance and voltage, if either or both are raised the energy density will be improved. In the following equation we have the energy density (E), specific capacitance (C), charge density (Q), and voltage (V) [109]:

$$E = \frac{CV^2}{2} = \frac{QV}{2} \qquad (3.1)$$

The power density of a supercapacitor defines how fast it can be discharged and depends on the voltage and the equivalent series resistance; the latter is to be kept to a minimum for high power density. We introduce the power density (P) and equivalent series resistance (R_s) [109]:

$$P = \frac{V^2}{4R_S} \qquad (3.2)$$

Supercapacitors can be classified into three types as shown in Figure 3.1. Electrochemical double layer capacitors (EDLC), pseudocapacitors and a mix of EDLC and pseudocapacitance called hybrid capacitors.

The EDLC supercapacitor has a very high-power density because it mainly stores its energy electrostatically, utilizing the double layer. Storing energy in this fashion, the supercapacitors can be charged and recharged for over 10^5 times and in theory infinite numbers. The downside of this storage mechanism is that the energy density is much lower compared to batteries. Batteries on the other hand have an energy storage based on Faradic charge transfer. A Faradic charge transfer is a charge that is transferred across an electric interface as a result of an electrochemical reaction [110]. The Faradic charge transfer can also be used as storage mechanism for supercapacitors and is called pseudocapacitance [110]. To enhance the energy density, abundant amount of research are ongoing on pseudocapacitive electrode materials.

Pseudocapacitance behaves like capacitance when characterized with voltammetry but occurs from an electrochemical reaction. The pseudocapacitance has been studied and tested for electrode materials using transition metals and electrically conductive polymers [111]. Both these methods show good result concerning energy density, but so far lack the number of charge-discharge cycles that can be sustained without serious detrimental impact on the device performance needed for it to utilize as supercapacitor electrode material in an IWS system as shown in Paper VI. Due to, so far a very limited number of life cycles for pseudocapacitors, a hybrid supercapacitor, might be a better solution [112].
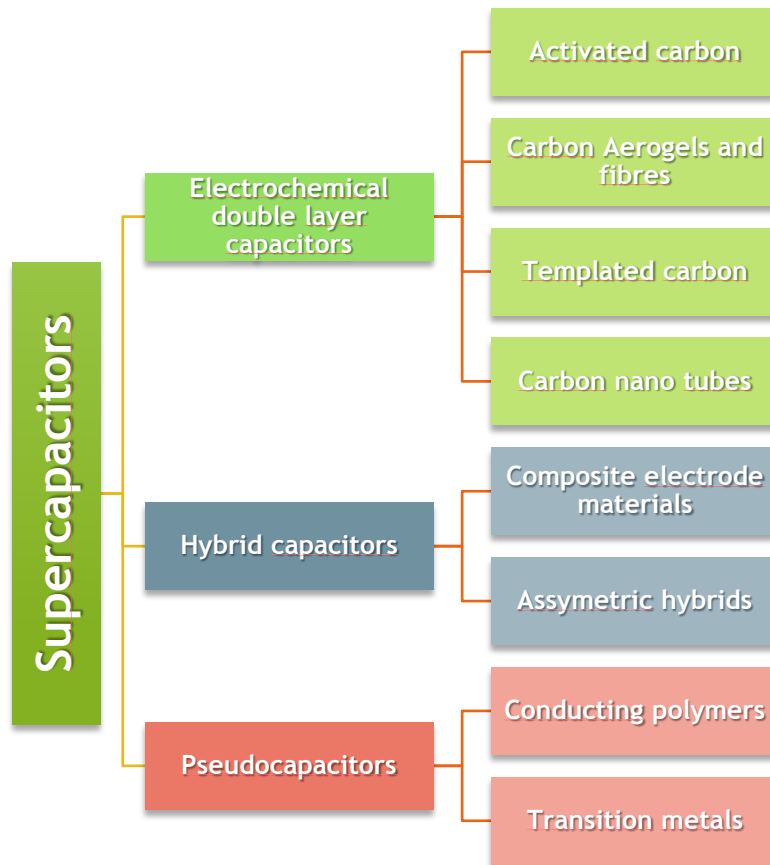
Figure 3.1 Classification of supercapacitors in three major groups EDLC, hybrid and pseudocapacitors with examples of electrode material for each group.

A hybrid supercapacitor has one half cell utilizing the double layer and the other half cell is based on pseudocapacitance. By that combination, the power density is higher compared to batteries and the energy density is higher compared to other types of supercapacitors [112].

Even though supercapacitors have inferior instantaneous energy density, over time with their huge cyclability, over their life time the supercapacitors can provide more stored energy than batteries can, shown in Table 3.1 from Paper VI. The life cycles for supercapacitors are 10^5 and higher and during the life time of an IWS system with an energy harvester this high number of cycles is needed

since the supercapacitor will be charged and recharged continuously with intermittent harvested energy.

	Supercapacitor	Battery LiPo
Wh/kg per cycle	9	250
Maximum number of cycles	100000	1000
Accumulated energy density for total number of cycles	900000	250000

Table 3.1 Energy density accumulated over the number of charge cycles shows that supercapacitors will deliver a higher energy density of nearly 4 times over time versus batteries. The approximation for the battery is overestimated since it does not take into account that the battery energy density decreases over time due to loss of active electrode material [113].

3.2 ELECTRODE MATERIALS FOR SUPERCAPACITORS

The commercial EDLC supercapacitors are mainly using active carbon as electrode material today [114]. The main reasons are that of the low production cost and easy production techniques of activated carbon. In Paper VI recent years of carbon electrode material research in the literature is compared; by looking at surface area versus capacitance for different carbon allotropes, conclusions regarding what electrode materials look promising can be drawn (Figure 3.2). The black line is based on an ideal model carbon electrode material with maximum active area, which only considers the double layer. Every electrode material would have lower value regardless of their surface area and structure since the model material is perfect in that sense. The material with highest capacitance per gram is the group called composites of carbon. These materials are combinations of carbon allotropes that enhance the surface area or the structure or both and therefore have better performance. Three measured electrode materials have values above the model maximum, these electrode materials are either measured with 6 M KOH or 0.1 M Na_2SO_4 as electrolyte instead of 1 M KOH which the rest are characterized with or are combinations with materials that uses the pseudocapacitance mechanism. From a more detailed look at the composite materials, the most promising electrode material is made of N-doped graphene nanosheets, Paper VI. The N-doping makes a part of the storage mechanism change from double layer to pseudocapacitance, which makes the capacitance higher and therefore also the energy density higher. The structure of the material, by implementing graphene nanosheets, is that the surface area is greatly enhanced and accessible for the electrolyte. Hence, the way to develop new materials is either by aiming at a more ordered structure, or to enhance the energy density by implementing pseudocapacitance.

An electrode material suitable for a supercapacitor in an IWS with energy harvesting needs to fulfill the following conditions:

- Sufficient number of charge and discharge cycles without deterioration during the lifetime of the device.
- High value of capacitance per gram and per volume, hence a possibility to scale it down for usage in e.g. Micro Electrical Mechanical System (MEMS) IWS.
- A low self-discharge.

The high number of cycles is needed because the harvested energy comes discontinuously and thus constantly charges and the IWS periodically discharges the supercapacitor typically when transmitting data. The AIWS has to be operational for a long time and supercapacitor have more than 10^6 cycles and a life expectancy over 20 years [115], [116]. A high number of life cycles entails that the super capacitor will not be the crucial part of the AIWS functionality over time.

A high value of specific capacitance is needed when the IWS system is scaled down to MEMS size or if the sensor needs a high amount of energy and therefore the size and weight of the supercapacitors becomes an issue.

A low self-discharge is also needed if the IWS system is in standby and is not able to harvest energy for a longer period and also if the harvester delivers low power it is also critical to have low losses or no energy will be stored. If a wireless system can harvest energy more or less continuously, the self-discharge time for a supercapacitor will not be reached. If the system fails to harvest the self-discharge is between 5-60% over a period of two weeks [117].

As presented in Table 3.1 from Paper VI the amount of cycles presented for tested electrode materials, does not show the high amount of cycles needed for long time IWS usage. Many are also reporting high degradation of the capacitance compared the first to the last cycle measured, meaning that the electrode material might break down due to degradation. Therefor life cycle measurement is crucial to verify for new usable electrode materials.

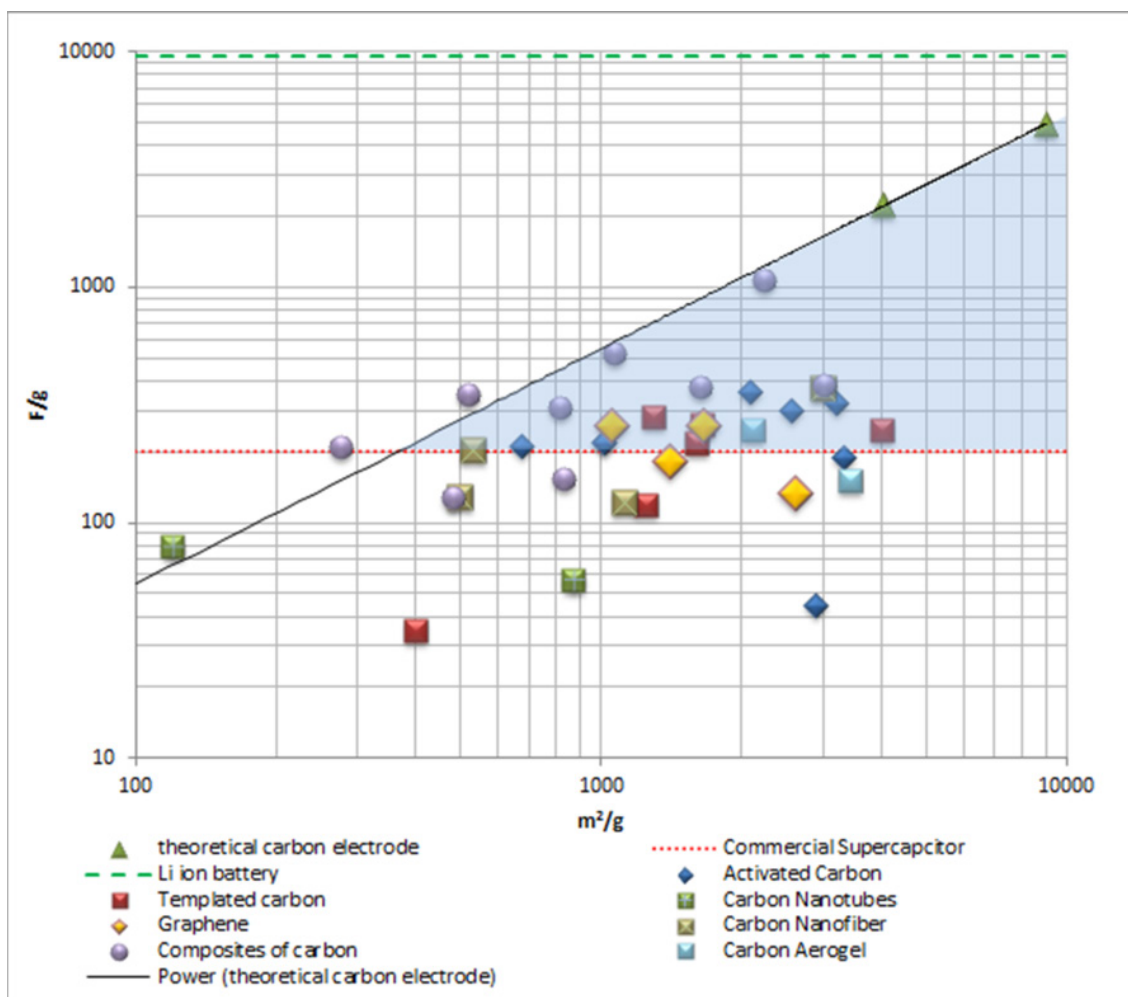*Figure 3.2 Capacitance per gram plotted against surface area per gram for electrodes with different carbon structures or composite carbon structures based on table 2.2, showing that a larger surface area doesn't necessarily give a higher capacitance. And that that electrode materials with pseudocapacitance or with a very well-ordered structure gives a higher capacitance with a smaller surface area, from Paper VI.*

Allotrope	Surface area m²/g	F/g	Electrolyte other than 1M KOH	Number of cycles	degradation
Composites of carbon	2231	1071		-	-
Composites of carbon	1059	524		-	-
Composites of carbon	3012	385		2500	-6%
Composites of carbon	1626	378		2000	-4,6%
CNF	3000	371		-	-
Activated carbon	2100	355		-	-
Composites of carbon	517	349	6 M KOH	5000	+8%
Activated carbon	3200	320		2500	-31%
Composites of carbon	810	310		1000	-3%
Activated carbon	2570	300		10000	-
Templated carbon	1295	284		-	-
Templated carbon	1650	260		-	-
Graphene	1050	258		2000	+1%
Graphene	1654	255		2000	-5,9%
Templated carbon	4000	250		10000	-2%
Carbon aerogel	2119	250		5000	-24%
Templated carbon	1600	220		-	-
Activated carbon	1012	218		1000	-3%
Composites of carbon	274	212	2 M KOH	2000	-16%
Activated carbon	674	210		-	-
CNF	529	202		3000	-3%
Activated carbon	3326	190		-	-
Graphene	1400	180		2000	-5,9%
Composites of carbon	830	154		1000	-20,4%
Carbon aerogel	3431	152		8000	-1%
Graphene	2600	132		1000	-14%
Composites of carbon	481	128		1500	-1%
CNF	500	128		100	-17%
CNF	1120	122		-	-
Templated carbon	1250	120		-	-
CNT	120	79	0,1 M Na2SO4	-	-
CNT	871	57		5000	-2%
Activated carbon	2900	44		-	-
Templated carbon	400	35		300	-2%

Table 3.2 Carbon allotropes compared by surface area, F/g, number of cycles and degradation, all crucial markers for a good electrode material suitable for supercapacitors in IWS systems (references are presented in Paper VI).

For the characterization of an electrode material for supercapacitors, one commonly used method is the three-electrode measurement. The three-electrode test cell contains a work-, counter- and reference electrode. The electrochemical performance of the electrode material is evaluated by cyclic voltammetry (CV) and galvanostatic charge-discharge (GCD).

CV studies the current response of the electrode material as a function of applied potentials [32]. The mass specific capacitance of the electrode from a CV is given by:

$$C = \frac{\int \frac{i dV}{m}}{v \Delta V} \qquad (3.3)$$

where i is the response current, ΔV is the electrochemical potential range of the CV, v is the potential scan rate and m is the mass of the electrode. The CV for an ideal EDLC electrode material is rectangular in shape and is marked with 1 (black dash dash dot line) in Figure 3.3. The current immediately switches sign when the potential sweep is reversed. The energy storage mechanism is here pure electrostatic. If there is resistance in the capacitor, the CV curve gets the shape marked by 2 (blue line) in Figure 3.3. And if the electrode material contains pseudocapacitative contributions the shape goes from rectangular to a deviation form marked as 3 (green dash line) in figure 3.3.

1. Ideal capacitor
2. Capacitor with resistivity
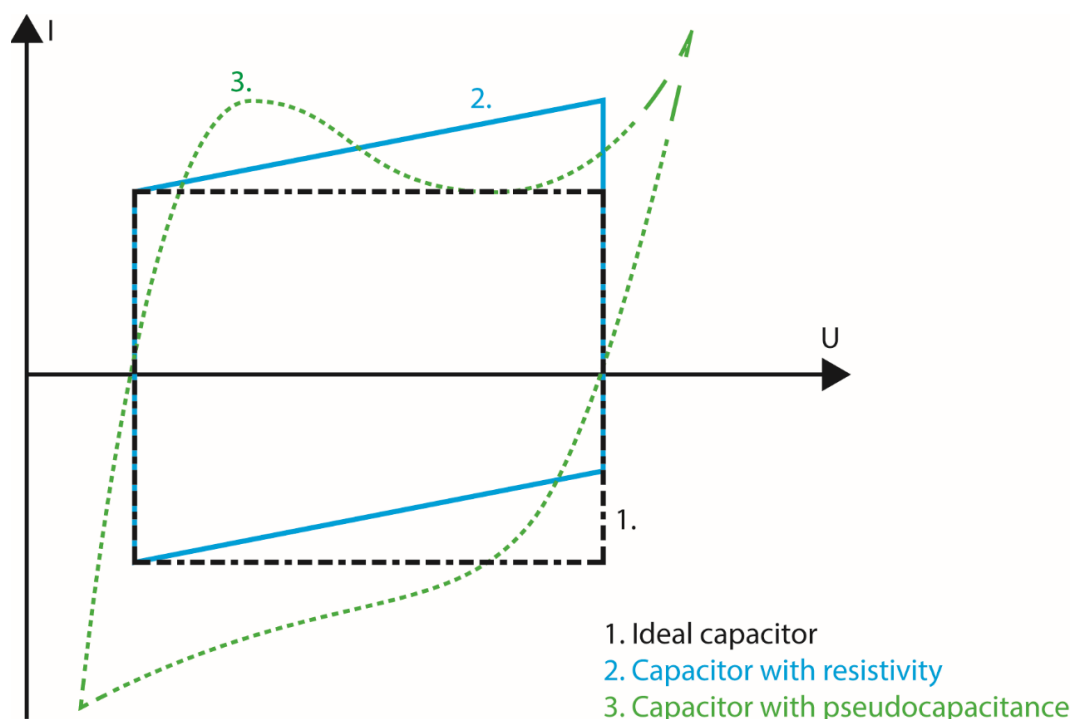3. Capacitor with pseudocapacitance

Figure 3.3 CV shapes for ideal EDLC electrode material and how the CV behaves when carbon is used as electrode material and the impact of redox reactions.

Cyclic charge discharge (CCD) studies the potential change for an electrode material as a function of time when a constant current is applied while charging and discharging [118]. The supercapacitor is charged at a constant current as presented schematically in Figure 3.4. The CCD curve is divided into two parts, first the charge of the supercapacitor and then the discharge. At the start of the discharge sequence there is a voltage change (V_{drop}) due to equivalent series resistance (ESR). In Figure 3.4 the dE is the change in voltage during discharge and dt is the discharge time.
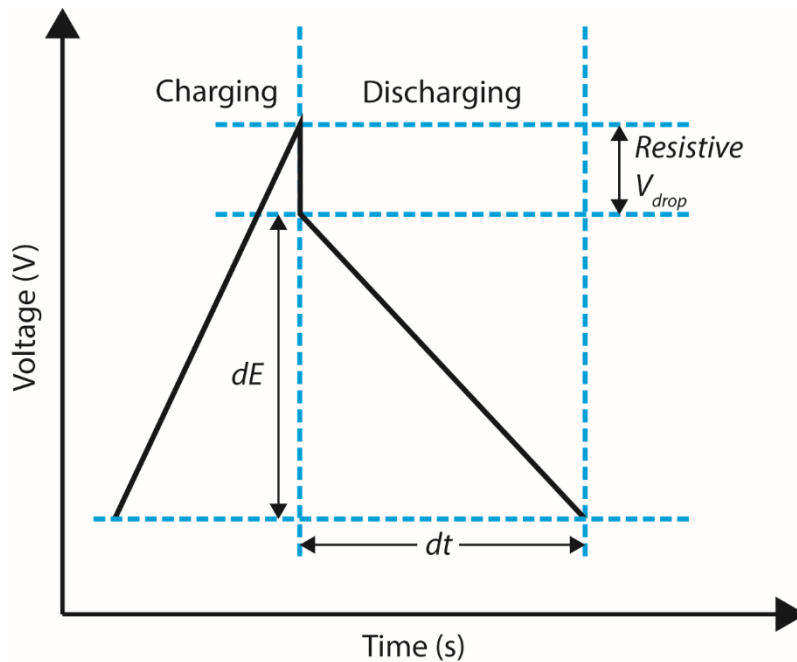
Figure 3.4 CCD schematically presented for an ideal electrode material.

The mass specific capacitance from CCD is calculated by:

$$C = \frac{i}{m(\frac{dV}{dt})} \qquad (3.4)$$

where i is the constant current and dV/dt is the slope of the discharge curve.

CV is used to characterize how the material behaves and if it is suitable as electrode material. CCD is used to see how the electrode material behaves after cycling or break down during cycling and how affected the material is by degradation. A good material suitable as electrode material needs to be stable while cycling where the degradation is kept to a minimum or ideally is nil between first to last cycle.

3.5.1 Electrode material structure and the impact of pores

As suggested in Paper VI, to ensure a high cyclability and to increase the energy density, new electrode materials based on composites of carbon allotropes and/or enhanced by pseudocapacitance are beneficial. A more well-ordered structure and enhancing the usable surface area is an indicated way to be able to obtain these better electrode materials. An important part of the structure is the pore distribution. There are three different types of pores in an electrode material: macro-, meso- and micro-pores. Macropores are above 50 nm, mesopores are between 2 – 50 nm and micro-pores are smaller than 2 nm [119] . The pores have different roles in the electrode material. Macropores add to the power density of the supercapacitor; however, macropores take a lot of valuable space, where more material could be built in. Mesopores add to the power density and since they are smaller than macro-pores they don't take as much place from the electrode material, hence they are better suited to carry the electrolyte in the electrode material [120]. The micropores are adding to the effective surface area where ions can attach to the electrode material [121]-[122]. Some carbon materials have very high densities of micro-pores, like carbon aerogel, but due to poor material structure many of these find themselves in closed cavities and can therefore not add to the active surface area [123]–[127]. A good electrode material has connected mesopore corridors with adjacent easily accessible micropores, a conjoined carbon on carbon electrode material can be fabricated with these traits.

3.5.2 Cellulose based carbon nanofibers

Carbon nanofibers (CNF) constitute a fascinating material and can be made from several different sources. Cellulose is a source that is renewable and environmental friendly [128]–[130]. Cellulose based CNF is made from cellulose acetate (CA) which by electrospinning can give fibrous mats. In this thesis the mats were placed in 50 ml of 0,1 M water solution of NAOH so the CA is hydrolyzed into regenerated cellulose. After carbonization, the fibrous mats consist of thin CNF with well-ordered mesoporous structure as presented in Figure 3.5. The CNF fibers have a diameter from tens of nanometers up to several hundred nanometers. From a supercapacitor perspective, as electrode material, CNFs have a fairly high surface area with a good, stable charge and discharge cycle life-time [131]–[134] and mechanical stability.
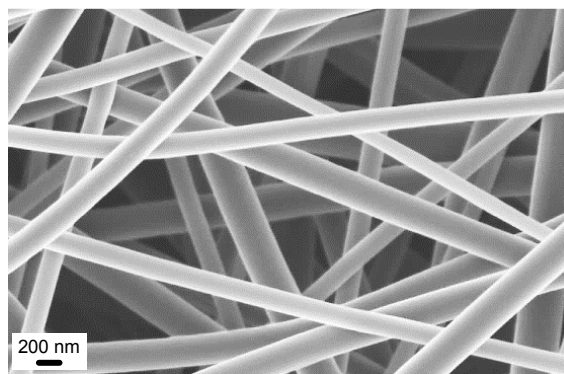

Figure 3.5 SEM image of CNFs.

3.5.3 Carbon nanotubes

Carbon nanotubes (CNT), are in this thesis made by chemical vapor deposition (CVD), cylindrical nanostructures [135]. These cylindrical structures have a wrapped graphene sheet as wall. The CNTs are on the nanometer scale and their diameter is ranging from $1 - 20$ nm. CNTs can be single walled, double walled or multiwalled. CNTs have good thermal and electrical properties, which make them suitable for being an electrode material in supercapacitors. To increase the effective surface area, CNTs can be grown vertically aligned in a dense pattern [118], [136], [137].

3.5.4 Conjoined carbon electrode material

Two different carbon allotropes can be merged together in pursuit of an increased specific capacitance. In Paper VII we investigated cellulosed CNF as base structure for CVD CNTs. CNF has a well-ordered structure with a large amount of mesopores for electrolyte transportation. CNT, due to the small diameter, has a higher effective surface area compared to the CNF. In Paper VII, CNTs are CVD grown on CNF. In Figure 3.6 the clearly visible border between pure CNF and CVD grown CNT on CNF is presented. Figure 3.7 present TEM images of the CNTs at different magnifications, where Figure 3.7 A shows a close look at a single CNT grown on one CNF fiber. Figure 3.7 B reveals that some catalytic particles are inside the CNT closer to the base than the tip. Figure 3.7 C shows that the CNTs are multiwalled. By conjoining CNF and CNT, the surface area is increased 3 times (Table 3.3). The capacitance is nearly doubled for CNF/CNT compared to CNF and the retention loss is only -3.4 % after 2000 cycles.

Sample	Surface area (m^2/g)	Electrode capacitance (F/g)	Capacitance retention $(\%)$
CNF	45	46.5	88.7
CNF/CNT	131	91.5	96.6

Table 3.3 Presenting data for the difference between pure CNF and CNF/CNT. Capacitance retention given after 2000 cycles.

Figure 3.6 SEM image of the border between pure CNF and CVD grown CNT on CNF
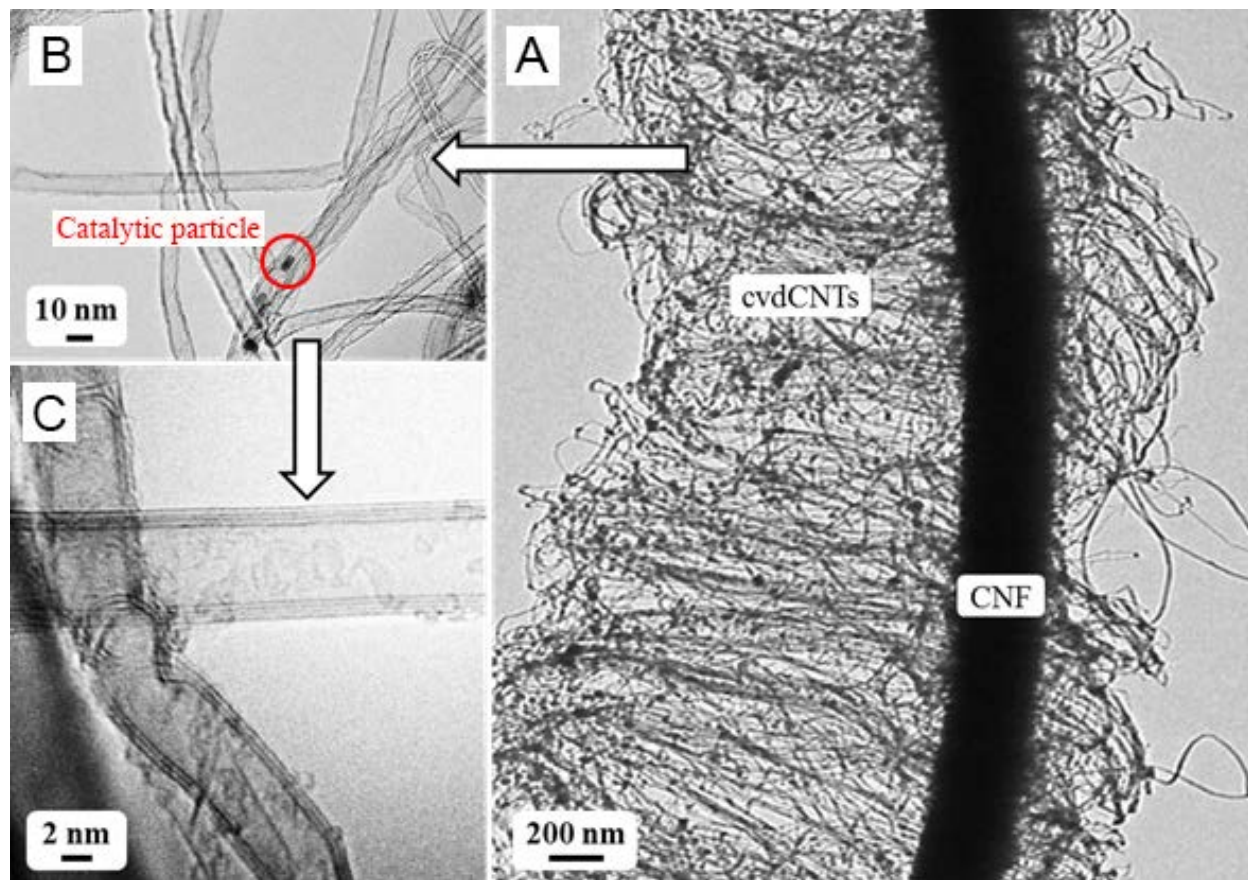
Figure 3.7 TEM images of CVD grown CNT on CNF.

As presented in Paper VII, the surface area of 131 m^2/g is rather low but still yields a specific capacitance of 91 F/g and placed in the model in Paper VI, the result is above the theoretical material. Compared with CNT and CNF, CNT are reported to have 79 F/g with a surface area of 120 m^2 [137] and activated CNF is reported to have 370 F/g with a surface area of 3000 m^2 [138] (Table 3.2). CNF/CNT compared to activated CNF, has a small surface area. Compared with electrode materials in Table 3.2, the low surface area indicates that the capacitance result is good, by merging these two carbon materials together. The structure of CNF is well-ordered which makes wetting easy for the electrolyte. Denser structure for the CNF will yield more area to grow CNT and increase the effective area of the CNF/CNT and the capacitance further.

The cycling stability, where degradation decreases and flattens out (presented in Paper VII), indicates that CNF/CNT will have the lifetime of 10^6 cycles desired for a supercapacitor in an IWS system.

Activated carbon is cost effective and is mainly used today for commercial supercapacitors. Tailored electrode materials are a better choice from an energy density perspective, but are more expensive to produce. Compared to active carbon they are not dependent on binders and conductive agents to work as an electrode material. The tailored electrode material like conjoined CNF/CNT

- 39 -

has also the advantage of an effective surface area, easily accessible for ions. This structural control is a beginning of making efficient electrode materials with high energy density. Conjoined carbon electrode materials, in the long run, show tremendous promise in outperforming todays commercial electrode materials in supercapacitors.

4 ENERGY HARVESTING ON GAS TURBINES

This chapter will present measurements in an authentic commercial test environment on a gas turbine. Challenges will be presented along with solutions both published and not published. At the end a complete IWS system powered by energy harvesting is demonstrated.

4.1 ENERGY HARVESTING ON GAS TURBINES

The importance of health monitoring on a gas turbine is significant from an environmental point of view. By better sensing the safety margins in a gas turbine used currently can increase and performance rises. For example, 10 °C uncertainty on the turbine entry temperature can have an impact on fuel consumption by 0,2 % and a change in the turbine tip clearance by 0,2 mm has an impact on the fuel consumption by 0,4 %. By more accurate sensing technology over 1,5 million tonnes of CO_2 could be saved [139]. Further health monitoring applications are gearbox sensing and strain/stress sensing on the attachment between the wing and the gas turbine. Today these sensors are cabled, the advantages of using an intelligent wireless sensor on a gas turbine is the removal of cabling and contacts for these.

4.2 HARVESTER OUTPUT ON GAS TURBINES, CHALLENGES

The environment close to a gas turbine contains; heat and vibrations. Both these ambient energies can be converted by harvesters, however both also are challenging to master when energy is to be converted. The heat around and close to a gas turbine during the combustion and exhaust sections, shown in Figure 4.1, are above 400 °C which is too high for a piezoelectric harvester and the circuits used for power management, measurements and transmission. Therefore, a piezoelectric energy harvester has limitations regarding its placement. At the air intake section, the gas turbine has much lower temperatures, which is more suitable for a piezoelectric energy harvester to be placed. The other challenge, vibrations might at first glance seem to be contradictive, since the piezoelectric energy harvester are to convert vibrations to electricity. However, the power density spectrum (PSD) for a gas turbine contains a wide spread of frequencies and high values of accelerations. For vibration harvesting two major challenges arises;

- Cabling between harvester and circuits
- Placement of harvester on the gas turbine which have an impact on the energy harvester output

The cables within the IWS needs to be properly attached and have multiple cores as presented in Figure 4.2. Multicore cables damp the vibrations in the cable hence the strain on soldered ends, which to our experience tends to break for single core cables.
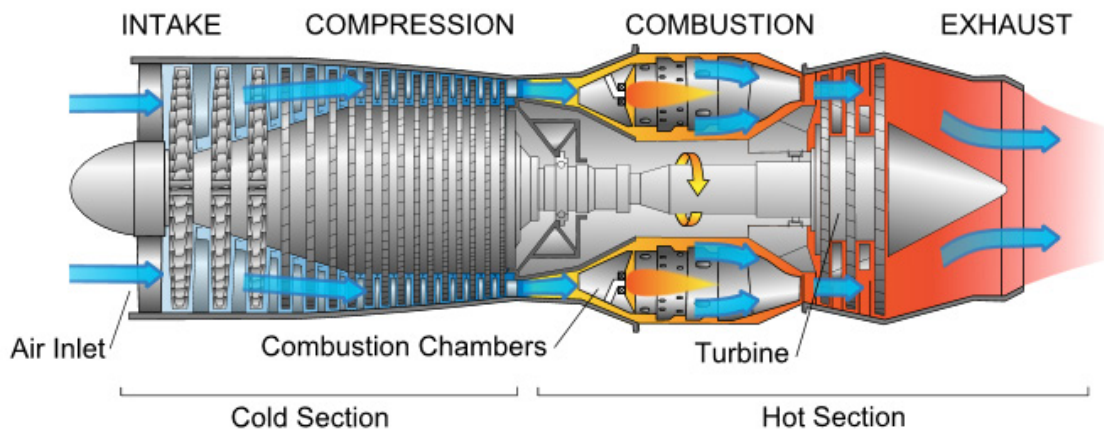
Figure 4.1 Schematic of a gas turbine, where the cold section is to the left where piezoelectric energy harvesters are more suitable and to the right the hot section where thermal harvesters are more suitable [140], [141].
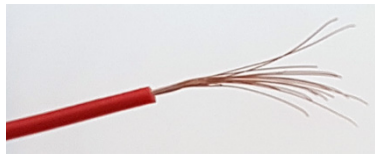
Figure 4.2 Multicore cable usable in harsh vibration environment.

The placement of the harvester on the gas turbine is an important issue to take under consideration. On a test site the gas turbine is attached to a dampening frame. Hence placing the harvester on that frame is futile due to damping. As presented in Figure 4.3 the box containing the harvester is strapped closely to the gas turbine by plastic zip ties. This solution is not a viable option for long term usage on test sites and plastic zip cords also has a damping effect via the transition between the gas turbine and the boxed harvester but it is easy to apply and considered good enough.

Figure 4.3 Boxed harvester attached to the mounting frame for the gas turbine by zip ties.

Considering only the placement of the harvester on the gas turbine, have in some cases a large negative impact on the output of the harvester. Presented in Figure 4.4 is a tuned backfolded harvester with output measured on a shaker table during a frequency sweep 50 to 400 Hz with actuation amplitude of 0,2 g. The same tuned harvester showed a different output when put on a gas turbine, presented in Figure 4.5. This is an example where the placement and the harvester axis direction have an impact of the output. The difference be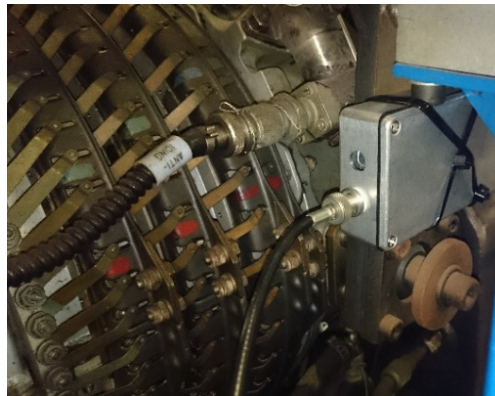tween the two measurements can be explained by looking at the three first modes of the backfolded harvester. In Figure 4.6 the three first modes are presented, where the first two modes are along the Y axis, while in the third mode is along the Z axis. The gas turbine on the test site is fixed to a frame, which is attached to the floor. By this fixture the vibrations from the gas turbine is damped inline with the Y axis. Calculated voltage output from simulations in COMSOL, presented in Table 4.1, shows that there is electric output for all three modes. Because of the gas turbine fixture with its damping on the Y axis it is reasonable to believe that the output from the harvester only is obtained for the third mode, as shown by the measured values in Figure 4.5.
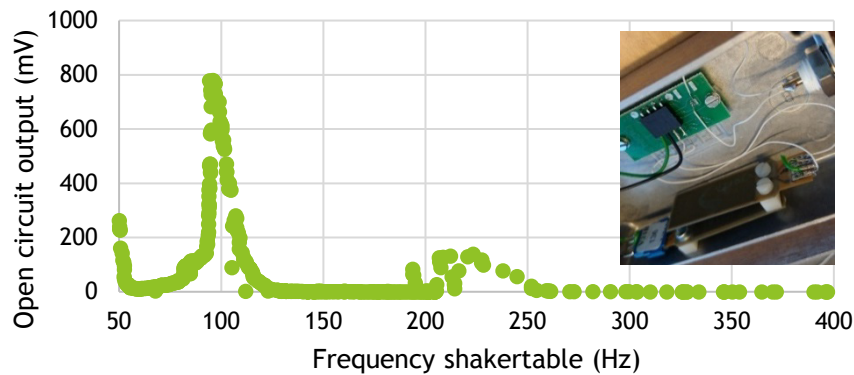
Figure 4.4 Open circuit voltage output from a backfolded harvester (inlet picture) on shaker table.
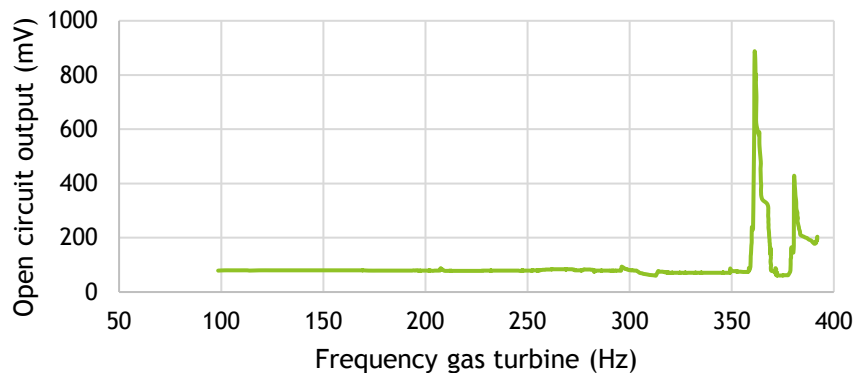
Figure 4.5 Open circuit voltage output from a backfolded harvester on a gas turbine.

Eigenfrequency	Output voltage (V)
114	3,3
191	3,3
456	3,2

Table 4.1 Tabulated COMSOL calculated open voltage for the three first eigenfrequencies on the backfolded harvester with 1g.

Mode 1

Mode 2

Mode 3
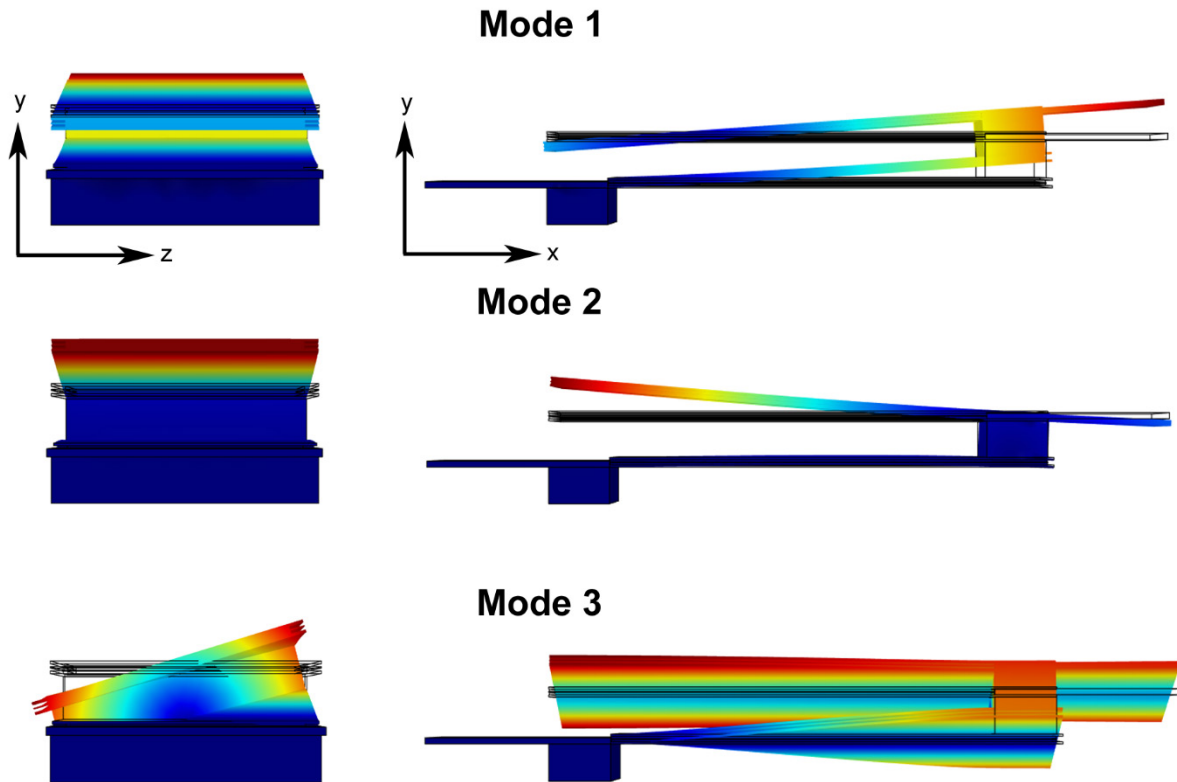
Figure 4.6, The three first modes of the backfolded harvester is presented. Mode 1 and 2 are under impact from vibrations in y axis, while the third mode is moving along the z axis.

4.3 CHARGING OF SUPERCAPACITORS BY HARVESTED POWER

The choice of supercapacitor as energy storage in an IWS is based on a life cycle perspective as presented in Paper VI. To be able to use the supercapacitor the difference between batteries and supercapacitors has to be examined. Batteries have an internal chemical potential difference between the electrodes with a charge transfer that creates an output voltage. While charging and discharging the voltage is relatively constant as presented schematically in Figure 4.7.
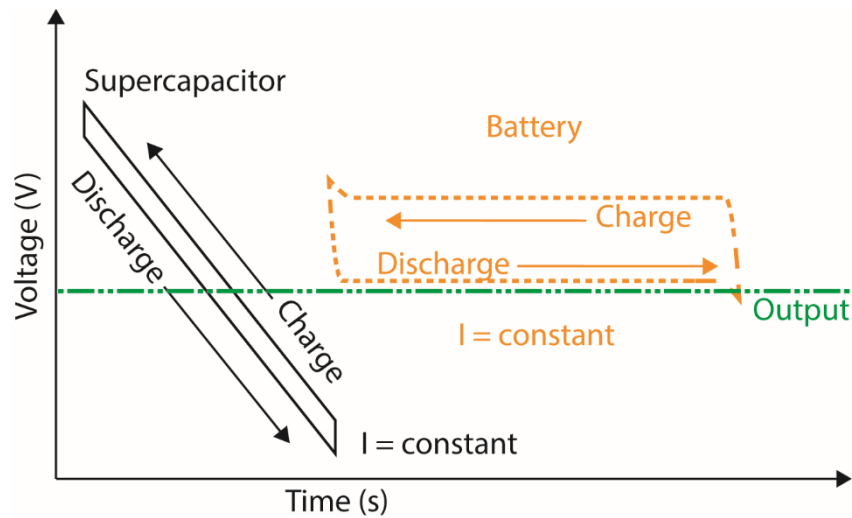
Figure 4.7 Schematic of battery and supercapacitor ideal charge and discharge.

The EDLC supercapacitor (in this thesis) stores the energy electrostatically and when charged the voltage increases linearly and during discharge the voltage decreases linearly as presented schematically in Figure 4.7. To be able to deliver energy to the sensor and Wi-Fi transition a power management module is needed. In this thesis a MIDE EHE004 is used. To be able to deliver energy, the power manager charges the supercapacitor up to the V_{in} rising voltage limit, presented in Figure 4.8. And when the V_{in} rising voltage limit is reached, EHE004 delivers energy until the V_{in} falling voltage limit is reached, as presented in Figure 4.8. The energy density for a battery is much higher compared to a supercapacitor. Due to the supercapacitor linear discharge behavior compared to the constant discharge behavior of batteries, energy density difference is increased, presented schematically in Figure 4.7 by the green dash-dot-dot line. The whole constant discharge from the battery is above the output line while half of the discharge from the supercapacitor is above the output line.

The Wi-Fi startup sequence for the used RF interface ZigBee is the most single power consumption task for the IWS system. The supercapacitor needs to have enough power for a startup sequence of 8 mW. This is achieved by a 20 mF supercapacitor. However, a 20 mF supercapacitor takes a long time to charge when a harvester is used, up to 3 hours even from an optimized harvester on the shaker table. This is because the current is not constant and the power from the harvester comes in small chunks. In Figure 4.8 the difference between ideal charge and harvester charge is demonstrated schematically. The charge time with power from the harvester, blue dash-dot-dot line in Figure 4.8, becomes logarithmic in nature and reaching the V_{in} rising level for the power management takes very long.
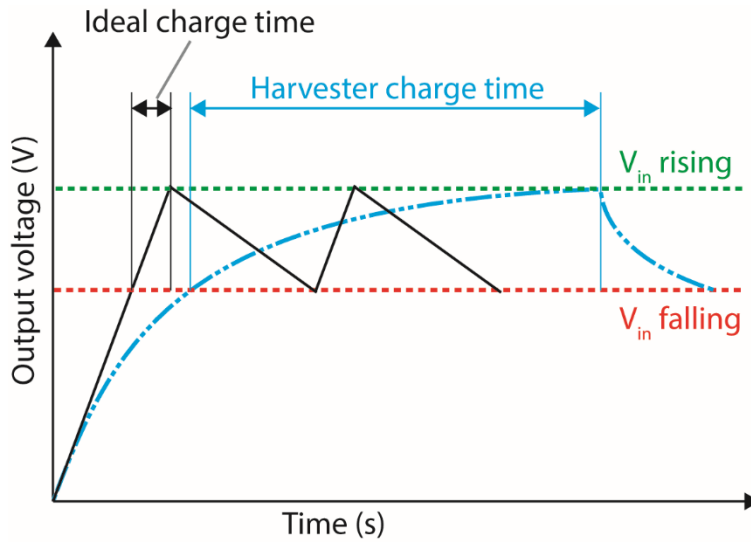
Figure 4.8 Schematic of difference in charge time and behavior between ideal charge and harvester-based charge of a supercapacitor.
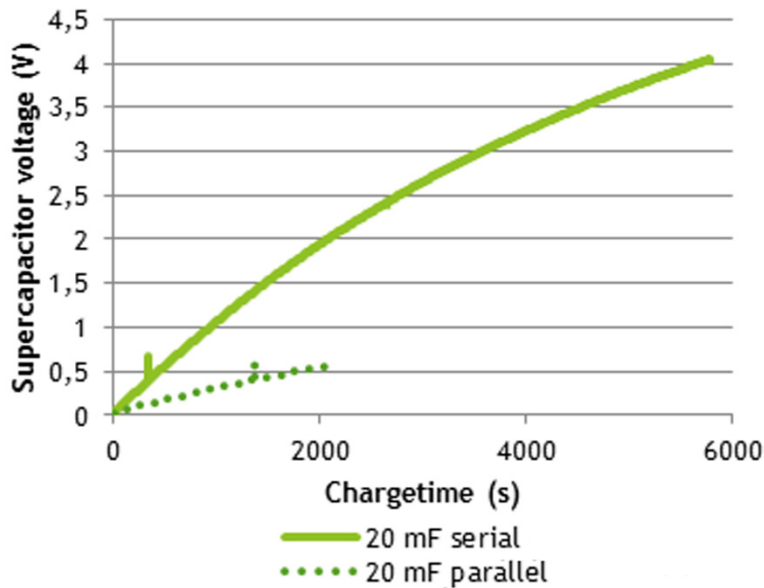
Figure 4.9 Demonstrated difference of charge time for two 20 mF supercapacitors connected serial and parallel.

To counter the charge time problem the supercapacitors were connected in series. In Figure 4.9 two 20 mF supercapacitors were connected in series and in parallel to demonstrate the difference in charge time. The two 20 mF connected in series (green solid line Figure 4.9), charge much faster compared to the two in parallel (dotted line Figure 4.9). However, connected in series the total capacitance is decreased, which was solved by using larger supercapacitors to have enough energy

to start up the Wi-Fi. In this thesis four 320 mF supercapacitors are connected in series, with a total capacitance of 80 mF. Connected in series, in the critical zone between start voltage and cut off voltage, a near linear behavior is achieved, presented with a black line in Figure 4.10 between V_{in} rising and V_{in} falling. By this solution the charge time is decreased considerably from up to 3 hours down to 1 minute on a shaker table.
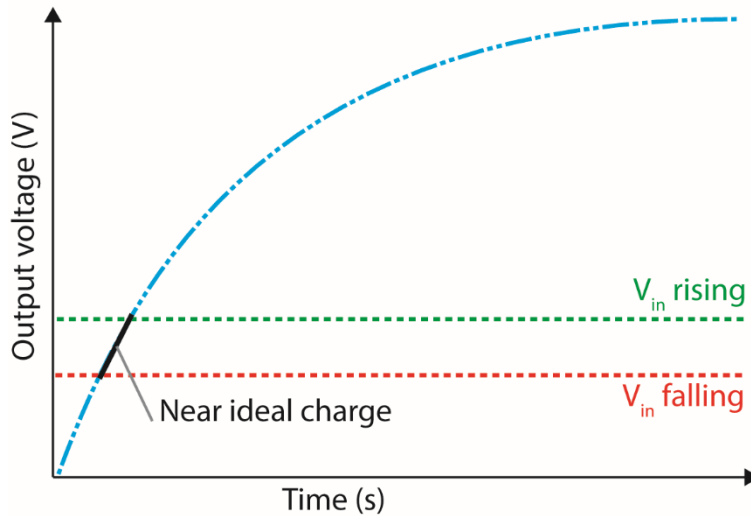
Figure 4.10 schematic of output voltage from supercapacitors connected in series where the charge from the harvester shows a near ideal behavior in the voltage window between V_{in} rising and V_{in} falling

4.4 WIRELESS INTELLIGENT SENSOR SYSTEM TEST ON A GAS TURBINE

There are many challenges that you encounter when you are to harvest energy to power a wireless sensor system on a gas turbine. The biggest challenge turned out to be to cover the right frequencies since there is an amount of many different resonances, in different directions on a gas turbine. In my case, in this thesis this occurred because we were not able to put the harvester directly on the gas turbine itself. In the end we found a protruding rectangular metal plate where the harvester could be attached. The protruding rectangular metal plate itself has an eigenfrequency, which naturally shifted, when the package with the harvester was attached to it. In the end an array of harvesters was used to be able to cover the wide range of possible frequencies where energy could be harvested, due to limited time access of the gas turbine, this turned out to be the quickest and best solution from a harvesting perspective.

The harvester was screwed directly to the protruding rectangular metal plate, depicted in Figure 4.11. Shown in Figure 4.11 is also the Wi-Fi transmitter (ZigBee), the power management module (EHE004) and the supercapacitor pack containing four 320 mF connected in series. After some on-site tweaking, the supercapacitor was charged from 0 V to 5,13V within 3,5 minutes. Which is a reasonable time, considering that under normal conditions the supercapacitor will be above 0 V

when power is starting to be harvested. In figure 4.12 the supercapacitor voltage under continuously transmitting power consumption is presented; the red ring indicates the startup sequence power consumption for the Wi-Fi transmitter. During harvesting the ZigBee was powered for 67 seconds, while broadcasting continuously.

Analyzing the supercapacitor voltage output data, a scenario for transmitting with 0 - 10 second interval was calculated (Figure 4.13). The result was that the harvester would be able to power the ZigBee if the ZigBee was broadcasting with 1 second interval. The specified demand was to transmit gearbox health data every 10 second, as discussed in Paper VIII, which by this demonstration is achieved. I believe that wireless sensors are very useful on test sites and later also on gas turbines mounted on airplanes. To be able to have a more effective output from the harvester its placement and attachment would be taken into consideration when designing new harvester and gas turbines.
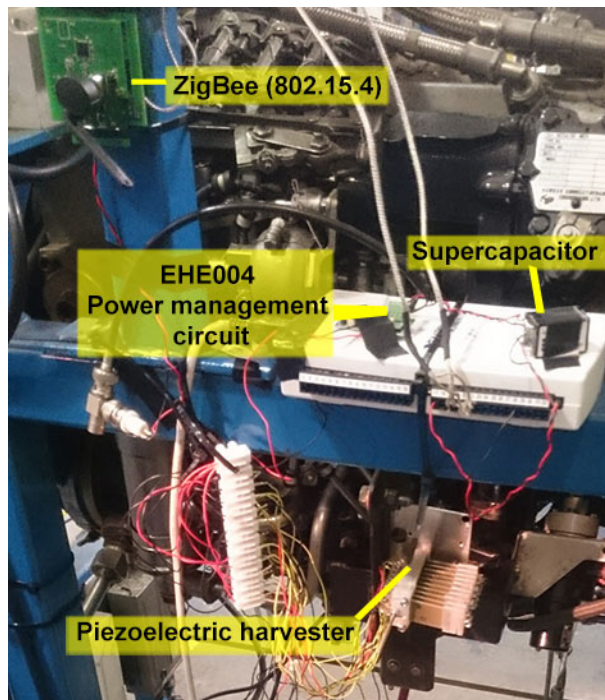

Figure 4.11 The final setup up components where the harvester was able to provide sufficient energy to power the wireless system.
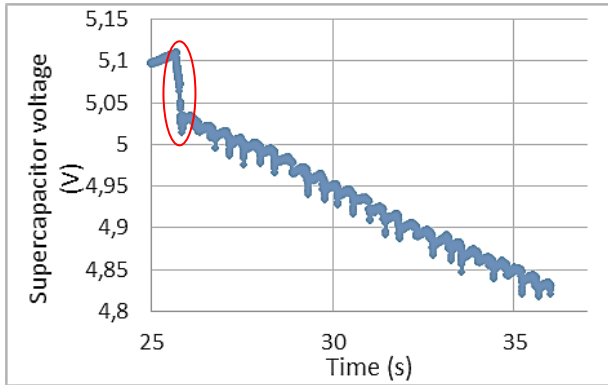
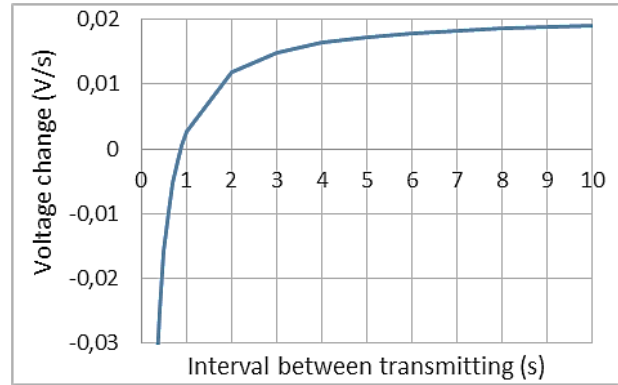*Figure 4.12 Supercapacitor voltage during startup (red circle) and continuously transmitting.*

Figure 4.13 Voltage change due to Wi-Fi transmition interval. Broadcasting every second will be possible since the net harvested energy is positive.

5 CONCLUSIONS

In this thesis, I have focused on two vital components in an AIWS, the energy harvester and the energy storage. The choice of energy harvester in this thesis cover piezoelectric cantilevers. Since my main application, gearbox surveillance on gas turbines, vibrations are an ambient source of energy due to placement on the gas turbine. Energy harvesting by heat conversion is not covered in this thesis. For the energy storage component, the choice in this thesis was supercapacitors, since they can be charged and discharged over 10^5 times, which is vital to be able to power an IWS over many years. To be able to utilize energy harvesting as an alternative or in combination with an energy storage it needs to be broadband, yield a sufficient power supply, have a reasonable size, which utilize available space to the fullest.

In the second chapter of this thesis I presented vibrational piezoelectric harvesting and the main challenge of obtaining a broad bandwidth and a maintained power output. To solve these challenges, I presented two macro harvesters and one MEMS harvester.

The first macro harvester, called backfolded, with two conjoined cantilevers, has a higher output compared with two single cantilevers. The backfolded also has two output peaks with maintained power output. The main reason for this effect is that the bottom cantilever has an extended stress distribution over the whole cantilever and therefore it is more effectively utilized compared to a cantilever attached in one end. Conjoining two cantilevers vertically on top of each other, compared to traditional 2DOF in one plane, gave higher energy output and I showed that it is possible to decrease the gap between the two output peaks, introducing length asymmetry. By achieving this, a broader bandwidth is obtained. The backfolded structure also is space-effective compared to other piezoelectric solutions with the same power output.

The second macro harvester, called self-tuning harvester with a sliding mass, is made up of two piezoelectric beams placed on top of each other with a connecting center beam between them. This design maintained the positive trait of extended stress distribution for both piezoelectric cantilevers, compared to the backfolded harvester where only the bottom cantilever achieved this trait. A broad bandwidth of 12 Hz is achieved by the mechanical self-tuning phenomena of sliding mass, the position of which on the middle beam changed the eigenfrequency of the system in total. In order to achieve broader bandwidth (37 Hz) with maintained power output (150 mW) the solution was to use asymmetric lengths of the piezoelectric cantilevers. The asymmetric solution was predicted by a numerical model of the system. In Paper IV the numerical model prediction was verified and examining one measured case closely, the sliding mass movement prediction correlated well with measurements.

The micro size harvester is also utilizing the trait of extended stress distribution by conjoining cantilevers. Here the cantilevers are in one plane with two outer cantilevers connected to a backfolded cantilever in the middle. This design is due to MEMS fabrication reasons, where a planar structure is easier to fabricate in contrast to a design where the cantilevers are on top of each other. Utilizing as much of the available device area as possible for harvesting is a crucial benefit

for conjoining cantilevers with extended stress distribution. This will make harvesters more space efficient and non efficient to be used in real life applications.

In this thesis I have schematically shown the difference between harvester other solutions and my solutions to achieve broader bandwidth and maintained power output. The reason I choose not to compare numbers is twofold; the absence of a standard FOM and wanting to clearly show the difference between my solutions and other solutions in the literature. Regarding the FOM, so far many have tried to create one, but the result is up to now that there are many different FOMs [64]. In order to benchmark my harvesters, I used an effective bandwidth, which was defined from the power I needed to provide for the IWS. I am aware that this need differs from application to application, but so is the design and tuning of the piezoelectric harvesters depending on where they are used. This implies that it is hard to compare different harvester solutions straight off. In the end the harvesters that can provide sufficient power will be the ones that we might be able to create a FOM from.

In the third chapter I presented that the best energy storage for IWS are supercapacitors. Compared to batteries, supercapacitors have a much longer life cycle, but inferior energy density, which shifts over the life time in favor for supercapacitors due to their high amount of charge and discharge cycles. To solve the challenge of the energy density, new electrode materials have to be developed. One such material is CNF conjoined with CVD grown CNT. This material provides positive traits such as a well-ordered structure with large amount of mesopores. The reported active surface area is 131 m^2/g and the capacitance is 91 F/g (without activation, which would yield a higher F/g)

The fourth chapter is dedicated to measurements in an authentic commercial test environment on a gas turbine and the challenges you encounter when to harvest energy on a gas turbine. The live test was finally successful after solving the following challenges:

- Cables breakage, due to ambient vibrations.
- Placement of the harvester.
- Charging supercapacitors.

The final goal was to show that it was possible to charge a supercapacitor within a reasonable time and provide harvested power for the IWS to broadcast data every 10 seconds. Both conditions were achieved while harvesting on a gas turbine. I am sure that autonomous IWS will be used more on various applications in the future. The development of harvesters is in its infancy, but it goes fast in the right direction with broader bandwidth and sufficient power. The development of ambient energy harvesters will have a positive impact on our environment, since we will be able to use less non-renewable resources for power and cables.

References

[1] M. ïngeles Serna, R. Casado, A. Bermïdez, N. Pereira, and S. Tennina, "Distributed Forest Fire Monitoring Using Wireless Sensor Networks," *Int. J. Distrib. Sens. Networks*, vol. 2015, pp. 1–18, Oct. 2015.

[2] A. Molina-Pico, D. Cuesta-Frau, A. Araujo, J. Alejandre, and A. Rozas, "Forest Monitoring and Wildland Early Fire Detection by a Hierarchical Wireless Sensor Network," *J. Sensors*, vol. 2016, pp. 1–8, Feb. 2016.

[3] X. Wu and D. W. Lee, "An electromagnetic energy harvesting device based on high efficiency windmill structure for wireless forest fire monitoring application," *Sensors Actuators, A Phys.*, vol. 219, pp. 73–79, Nov. 2014.

[4] M. Pellegrini, "Intelligent wireless sensor nodes in water monitoring systems," in *2014 IEEE Workshop on Environmental, Energy, and Structural Monitoring Systems Proceedings*, 2014, pp. 1–6.

[5] P. Giménez, B. Molina, J. Calvo-Gallego, M. Esteve, and C. E. Palau, "I3WSN: Industrial intelligent wireless sensor networks for indoor environments," *Comput. Ind.*, vol. 65, no. 1, pp. 187–199, Jan. 2014.

[6] M. S. Lebold, B. Murphy, D. Boylan, and K. Reichard, "Wireless Technology Study and the Use of Smart Sensors for Intelligent Control and Automation," in *2005 IEEE Aerospace Conference*, 2005, pp. 1–15.

[7] J. Lynch, "Monitoring the health of civil infrastructure with intelligent wireless sensors," *SPIE Newsroom*, pp. 352–356, 2009.

[8] A. Basharat, N. Catbas, and Mubarak Shah, "A Framework for Intelligent Sensor Network with Video Camera for Structural Health Monitoring of Bridges," *Third IEEE Int. Conf. Pervasive Comput. Commun. Work.*, pp. 385–389, 2005.

[9] V. Vaidehi, M. Vardhini, H. Yogeshwaran, G. Inbasagar, R. Bhargavi, and C. Sweetlin Hemalatha, "Agent based health monitoring of elderly people in indoor environments using wireless sensor networks," *Procedia Comput. Sci.*, vol. 19, pp. 64–71, Jan. 2013.

[10] Y. Cheng, F. Gao, A. Hanif, Z. Lu, and Z. Li, "Development of a capacitive sensor for concrete structure health monitoring," *Constr. Build. Mater.*, vol. 149, pp. 659–668, Sep. 2017.

[11] S. Das, P. Saha, and S. K. Patro, "Vibration-based damage detection techniques used for health monitoring of structures: a review," *J. Civ. Struct. Heal. Monit.*, vol. 6, no. 3, pp. 477–507, Jul. 2016.

[12] A. Vijayaraghavan and D. Dornfeld, "Automated energy monitoring of machine tools," *CIRP Ann. - Manuf. Technol.*, vol. 59, no. 1, pp. 21–24, 2010.

[13] Y. Hao and R. Foster, "Wireless body sensor networks for health-monitoring applications," *Physiological Measurement*, vol. 29, no. 11. 2008.

[14] L. F. Walubita, D. C. S. Djebou, A. N. M. Faruk, S. I. Lee, S. Dessouky, and X. Hu, "Prospective of societal and environmental benefits of piezoelectric technology in road energy harvesting," *Sustain.*, vol. 10, no. 2, p. 383, Feb. 2018.

[15] A. Vaughan, "Google uses AI to cut data centre energy use by 15%," *The Guardian*, 2016. [Online]. Available: https://www.theguardian.com/environment/2016/jul/20/google-ai-cut-data-centre-energy-use-15-per-cent. [Accessed: 27-Aug-2018].

[16] "Final Report Summary - STARGATE (Sensors Towards Advanced Monitoring and Control of Gas Turbine Engines) | Report Summary | STARGATE | FP7 | CORDIS | European Commission." [Online]. Available: https://cordis.europa.eu/result/rcn/187512_en.html. [Accessed: 03-Jun-2018].

[17] A. Othman, "Energy storage system options in Intelligent Wireless Sensor Network," in *ICMT 2017 - 6th*

International Conference on Military Technologies, 2017, pp. 772–778.

[18]   Y. Fan and J. Yu, "The Communication Protocol for Wireless Sensor Network about LEACH," in *2007 International Conference on Computational Intelligence and Security Workshops (CISW 2007)*, 2007, pp. 550–553.

[19]   A. S. Weddell, M. Magno, G. V. Merrett, D. Brunelli, B. M. Al-Hashimi, and L. Benini, "A Survy of Multi-Source Energy Harvesting Systems," *Des. Autom. Test Eur. Conf. Exhib. (DATE), 2013*, pp. 905–908, 2013.

[20]   O. Berder and O. Sentieys, "PowWow : Power Optimized Hardware/Software Framework for Wireless Motes," in *Proc. 23rd International Conference on Architecture of Computing Systems (ARCS)*, 2010, pp. 1–5.

[21]   Q. Ou, "Vibration-based Energy Harvesting for Wireless Sensors used in Machine Condition Monitoring," p. 54, 2012.

[22]   S. R. Jino Ramson and D. Jackuline Moni, "Applications of Wireless Sensor Networks - A survey," *Proc. IEEE Int. Conf. Innov. Electr. Electron. Instrum. Media Technol. ICIEEIMT 2017*, vol. 2017–Janua, pp. 325–329, 2017.

[23]   E. Popovici, M. Magno, and S. Marinkovic, "Power management techniques for Wireless Sensor Networks: A review," *5th IEEE Int. Work. Adv. Sensors Interfaces IWASI*, pp. 194–198, 2013.

[24]   I. F. Akyildiz, W. Su, Y. Sankarasubramaniam, and E. Cayirci, "A survey on sensor networks," *IEEE Commun. Mag.*, vol. 40, no. 8, pp. 102–105, 2002.

[25]   W. Rehan, S. Fischer, and M. Rehan, "Machine-learning based channel quality and stability estimation for stream-based multichannel wireless sensor networks," *Sensors (Switzerland)*, vol. 16, no. 9, 2016.

[26]   S. Mekid, "Further structural intelligence for sensors cluster technology in manufacturing," *Sensors*, vol. 6, no. 6, pp. 557–577, 2006.

[27]   J. E. Brignell, "Future of intelligent sensors: A problem of technology or ethics?," *Sensors Actuators, A Phys.*, vol. 56, no. 1–2, pp. 11–15, 1996.

[28]   K. Parajuly, K. Habib, C. Cimpan, G. Liu, and H. Wenzel, "End-of-life resource recovery from emerging electronic products – A case study of robotic vacuum cleaners," *J. Clean. Prod.*, vol. 137, pp. 652–666, Nov. 2016.

[29]   M. C. Kang, K. S. Kim, D. K. Noh, J. W. Han, and S. J. Ko, "A robust obstacle detection method for robotic vacuum cleaners," *IEEE Trans. Consum. Electron.*, vol. 60, no. 4, pp. 587–595, Nov. 2014.

[30]   J. P. Amaro, F. J. T. E. Ferreira, R. Cortesão, and J. Landeck, "Powering Wireless Sensor Networks Nodes for Complex Protocols on Harvested Energy," *Procedia Technol.*, vol. 5, pp. 518–526, Jan. 2012.

[31]   S. C. Lee and W. Y. Jung, "Analogical understanding of the Ragone plot and a new categorization of energy devices," *Energy Procedia*, vol. 88, pp. 526–530, Jun. 2016.

[32]   M. Inagaki, H. Konno, and O. Tanaike, "Carbon materials for electrochemical capacitors," *J. Power Sources*, vol. 195, no. 24, pp. 7880–7903, 2010.

[33]   A. Nedjalkov, J. Meyer, M. Köhring, A. Doering, M. Angelmahr, S. Dahle, A. Sander, A. Fischer, and W. Schade, "Toxic Gas Emissions from Damaged Lithium Ion Batteries—Analysis and Safety Enhancement Solution," *Batteries*, vol. 2, no. 1, p. 5, 2016.

[34]   L. L. Gaines and J. B. Dunn, *Lithium-Ion Battery Environmental Impacts*. 2014.

[35]   A. C. Miklos, C. Li, C. D. Sorrell, L. A. Lyon, and G. J. Pielak, "An upper limit for macromolecular crowding effects," *BMC Biophys.*, vol. 4, no. 1, 2011.

[36] L. Sun and K. Qiu, "Vacuum pyrolysis and hydrometallurgical process for the recovery of valuable metals from spent lithium-ion batteries," *J. Hazard. Mater.*, vol. 194, pp. 378–384, Oct. 2011.

[37] L. Li, L. Zhai, X. Zhang, J. Lu, R. Chen, F. Wu, and K. Amine, "Recovery of valuable metals from spent lithium-ion batteries by ultrasonic-assisted leaching process," *J. Power Sources*, vol. 262, pp. 380–385, Sep. 2014.

[38] L. L. Zhang and X. S. Zhao, "Carbon-based materials as supercapacitor electrodes," *Chemical Society Reviews*, vol. 38, no. 9. pp. 2520–2531, 2009.

[39] M. Winter and R. J. Brodd, "What are batteries, fuel cells, and supercapacitors?," *Chem. Rev.*, vol. 104, no. 10, pp. 4245–4269, 2004.

[40] J. R. Miller and P. Simon, "Materials science: Electrochemical capacitors for energy management," *Science (80-.).*, vol. 321, no. 5889, pp. 651–652, Aug. 2008.

[41] D. Miller, "Building a Project Work Breakdown Structure," *Electrochem. Soc.*, vol. 20085940, 2008.

[42] A. G. Pandolfo and A. F. Hollenkamp, "Carbon properties and their role in supercapacitors," *J. Power Sources*, vol. 157, no. 1, pp. 11–27, 2006.

[43] R. Kötz and M. Carlen, "Principles and applications of electrochemical capacitors," *Electrochim. Acta*, vol. 45, no. 15–16, pp. 2483–2498, 2000.

[44] B. Van Bavel, E. Buringh, and J. Dijkman, "Mills, cranes, and the great divergence: the use of immovable capital goods in western Europe and the Middle East, ninth to sixteenth centuries," *Econ. Hist. Rev.*, vol. 71, no. 1, pp. 31–54, Feb. 2018.

[45] E. K. Stigka, J. A. Paravantis, G. K. Mihalakakou, E. K. Stigka, J. A. Paravantis, and G. K. Mihalakakou, "Renewable & sustainable energy reviews.," *Renew. Sustain. Energy Rev.*, vol. 32, no. C, pp. 100–106, 2014.

[46] R. Torah, P. Glynne-Jones, M. Tudor, T. O'Donnell, S. Roy, and S. Beeby, "Self-powered autonomous wireless sensor node using vibration energy harvesting," *Meas. Sci. Technol.*, vol. 19, no. 12, p. 125202, 2008.

[47] A. Manbachi and R. S. C. Cobbold, "Development and application of piezoelectric materials for ultrasound generation and detection," *Ultrasound*, vol. 19, no. 4. pp. 187–196, 2011.

[48] E. Garber, "The Beginnings of Piezoelectricity: A Study in Mundane Physics," *Ann. Sci.*, vol. 67, no. 2, pp. 261–265, 2010.

[49] W. P. Mason, "Piezoelectricity, its history and applications," *J. Acoust. Soc. Am.*, vol. 70, no. 6, pp. 1561–1566, Dec. 1981.

[50] T. L. Jordan and N. Langley, "Piezoelectric Ceramics Characterization," *Contract*, p. 23, 2001.

[51] F. Lucarelli, S. Tombelli, M. Minunni, G. Marrazza, and M. Mascini, "Electrochemical and piezoelectric DNA biosensors for hybridisation detection," *Analytica Chimica Acta*, vol. 609, no. 2. pp. 139–159, 2008.

[52] S. Tombelli, M. Minunni, A. Santucci, M. M. Spiriti, and M. Mascini, "A DNA-based piezoelectric biosensor: Strategies for coupling nucleic acids to piezoelectric devices," *Talanta*, vol. 68, no. 3, pp. 806–812, 2006.

[53] A. E. Kaifer, "Fundamentals of Analytical Chemistry. Sixth edition (Skoog, Douglas A.; West, Donald M.; Hollar, James F.)," in *Journal of Chemical Education*, vol. 69, no. 11, 1992, p. A305.

[54] D. H. Walsh, "Electronics for Vehicle Safety in the Near and Intermediate Future," in *Vehicle Electronics in the 90's: Proceedings of the International Congress on Transportation Electronics*, 1998, pp. 165–168.

[55]   R. D. King-Smith and D. Vanderbilt, "Theory of polarization of crystalline solids," *Phys. Rev. B*, vol. 47, no. 3, pp. 1651–1654, 1993.

[56]   A. Vazquez Carazo, "Piezoelectric Transformers: An Historical Review," *Actuators*, vol. 5, no. 2, p. 12, Apr. 2016.

[57]   M. Birkholz, "Crystal-field induced dipoles in heteropolar crystals I: Concept," *Zeitschrift für Phys. B Condens. Matter*, vol. 96, no. 3, pp. 325–332, 1995.

[58]   H. Lu, C. W. Bark, D. Esque De Los Ojos, J. Alcala, C. B. Eom, G. Catalan, and A. Gruverman, "Mechanical writing of ferroelectric polarization," *Science (80-.).*, vol. 335, no. 6077, pp. 59–61, 2012.

[59]   S. Trolier-Mckinstry, "Crystal chemistry of piezoelectric materials," in *Piezoelectric and Acoustic Materials for Transducer Applications*, 2008, pp. 39–56.

[60]   Y. Zhang, H. Sun, and W. Chen, "A brief review of Ba(Ti0.8Zr0.2)O3-(Ba0.7Ca0.3)TiO3based lead-free piezoelectric ceramics: Past, present and future perspectives," *J. Phys. Chem. Solids*, vol. 114, pp. 207–219, Mar. 2018.

[61]   D. Damjanovic, "Ferroelectric, dielectric and piezoelectric properties of ferroelectric thin films and ceramics," *Reports Prog. Phys.*, vol. 61, no. 9, pp. 1267–1324, 1998.

[62]   S. P. Beeby, M. J. Tudor, N. M. White -, F. Lu, H. P. Lee, S. P. Lim -Topical Review Dibin Zhu, M. J. Tudor, S. P. Beeby -, N. M. White, and P. Glynne-Jones, "A novel thick-film piezoelectric micro-generator Related content Modeling and analysis of micro piezoelectric power generators for MEMS applications Recent citations A novel thick-film piezoelectric micro-generator," 2001.

[63]   S. Priya, H.-C. Song, Y. Zhou, R. Varghese, A. Chopra, S.-G. Kim, I. Kanno, L. Wu, D. S. Ha, J. Ryu, and R. G. Polcawich, "A Review on Piezoelectric Energy Harvesting: Materials, Methods, and Circuits," *Energy Harvest. Syst.*, vol. 4, no. 1, 2017.

[64]   R. Xu and S.-G. Kim, "Figures of Merits of Piezoelectric Materials in Energy," *PowerMEMS*, pp. 464–467, 2012.

[65]   L. Tang, Y. Yang, and C. K. Soh, "Toward broadband vibration-based energy harvesting," *J. Intell. Mater. Syst. Struct.*, vol. 21, no. 18, pp. 1867–1897, 2010.

[66]   O. Aldraihem and A. Baz, "Energy harvester with a dynamic magnifier," *J. Intell. Mater. Syst. Struct.*, vol. 22, no. 6, pp. 521–530, 2011.

[67]   A. Erturk, J. M. Renno, and D. J. Inman, "Modeling of piezoelectric energy harvesting from an L-shaped beam-mass structure with an application to UAVs," *J. Intell. Mater. Syst. Struct.*, vol. 20, no. 5, pp. 529–544, 2009.

[68]   M. Ferrari, V. Ferrari, M. Guizzetti, D. Marioli, and A. Taroni, "Piezoelectric multifrequency energy converter for power harvesting in autonomous microsystems," *Sensors Actuators, A Phys.*, vol. 142, no. 1, pp. 329–335, 2008.

[69]   L. Gu and C. Livermore, "Passive self-tuning energy harvester for extracting energy from rotational motion," *Appl. Phys. Lett.*, vol. 97, no. 8, p. 081904, Aug. 2010.

[70]   S. E. Jo, M. S. Kim, and Y. J. Kim, "Passive-self-tunable vibrational energy harvester," *2011 16th Int. Solid-State Sensors, Actuators Microsystems Conf.*, pp. 691–694, Jun. 2011.

[71]   D. Zhu, M. J. Tudor, and S. P. Beeby, "Strategies for increasing the operating frequency range of vibration energy harvesters: A review," *Meas. Sci. Technol.*, vol. 21, no. 2, p. 022001, 2010.

[72]   C. Eichhorn, F. Goldschmidtboeing, and P. Woias, "Bidirectional frequency tuning of a piezoelectric energy converter based on a cantilever beam," *J. Micromechanics Microengineering*, vol. 19, no. 9, p. 094006, Sep.

2009.

[73]   E. S. Leland and P. K. Wright, "Resonance tuning of piezoelectric vibration energy scavenging generators using compressive axial preload," *Smart Mater. Struct.*, vol. 15, no. 5, pp. 1413–1420, Oct. 2006.

[74]   S. Roundy and Y. Zhang, "Toward self-tuning adaptive vibration based micro-generators," *Smart Struct. Devices, Syst. II, Pt 1 2*, vol. 5649, pp. 373–384, 2005.

[75]   A. F. Arrieta, P. Hagedorn, A. Erturk, and D. J. Inman, "A piezoelectric bistable plate for nonlinear broadband energy harvesting," *Appl. Phys. Lett.*, vol. 97, no. 10, p. 104102, Sep. 2010.

[76]   F. Cottone, R. Mincigrucci, I. Neri, F. Orfei, F. Travasso, H. Vocca, and L. Gammaitoni, "Nonlinear kinetic energy harvesting," *Procedia Comput. Sci.*, vol. 7, pp. 190–191, 2011.

[77]   A. Erturk, J. Hoffmann, and D. J. Inman, "A piezomagnetoelastic structure for broadband vibration energy harvesting," *Appl. Phys. Lett.*, vol. 94, no. 25, 2009.

[78]   S. M. Shahruz, "Design of mechanical band-pass filters for energy scavenging," *J. Sound Vib.*, vol. 292, no. 3–5, pp. 987–998, 2006.

[79]   H. Xue, Y. Hu, and Q. Wang, "Broadband piezoelectric energy harvesting devices using multiple bimorphs with different operating frequencies," *IEEE Trans Ultrason Ferroelectr Freq Control.*, vol. 55, no. 9, pp. 2104–8, 2008.

[80]   M. Ferrari, V. Ferrari, M. Guizzetti, D. Marioli, and A. Taroni, "Piezoelectric multifrequency energy converter for power harvesting in autonomous microsystems," *Sensors Actuators, A Phys.*, vol. 142, no. 1, pp. 329–335, 2008.

[81]   S. Qi, R. Shuttleworth, S. O. Oyadiji, and J. Wright, "Design of a multiresonant beam for broadband piezoelectric energy harvesting," *Smart Mater. Struct.*, vol. 19, no. 9, p. 94009, 2010.

[82]   Y. Tadesse, Shujun Zhang, and S. Priya, "Multimodal energy harvesting system: Piezoelectric and electromagnetic," *J. Intell. Mater. Syst. Struct.*, vol. 20, no. 5, pp. 625–632, 2009.

[83]   Q. Ou, X. Chen, S. Gutschmidt, A. Wood, N. Leigh, and A. F. Arrieta, "An experimentally validated double-mass piezoelectric cantilever model for broadband vibration-based energy harvesting," *J. Intell. Mater. Syst. Struct.*, vol. 23, no. 2, pp. 117–126, 2012.

[84]   W. Zhou, G. R. Penamalli, and L. Zuo, "An efficient vibration energy harvester with a multi-mode dynamic magnifier," *Smart Mater. Struct.*, vol. 21, no. 1, p. 15014, 2012.

[85]   H. Wu, L. Tang, Y. Yang, and C. K. Soh, "A novel two-degrees-of-freedom piezoelectric energy harvester," *J. Intell. Mater. Syst. Struct.*, vol. 24, no. 3, pp. 357–368, 2013.

[86]   M. Lallart, S. R. Anton, and D. J. Inman, "Frequency self-tuning scheme for broadband vibration energy harvesting," *J. Intell. Mater. Syst. Struct.*, vol. 21, no. 9, pp. 897–906, Jun. 2010.

[87]   D. Guyomar and M. Lallart, "Recent progress in piezoelectric conversion and energy harvesting using nonlinear electronic interfaces and issues in small scale implementation," *Micromachines*, vol. 2, no. 2, pp. 274–294, Jun. 2011.

[88]   C. Eichhorn, F. Goldschmidtboeing, Y. Porro, and P. Woias, "A Piezoelectric Harvester with an Integrated Frequency-Tuning Mechanism," *PowerMEMS 2009*, no. Figure 3, pp. 45–48, 2009.

[89]   D. J. Morris, J. M. Youngsman, M. J. Anderson, and D. F. Bahr, "A resonant frequency tunable, extensional mode piezoelectric vibration harvesting mechanism," *Smart Mater. Struct.*, vol. 17, no. 6, p. 065021, Dec. 2008.

[90]   J. M. Youngsman, T. Luedeman, D. J. Morris, M. J. Anderson, and D. F. Bahr, "A model for an extensional

mode resonator used as a frequency-adjustable vibration energy harvester," *J. Sound Vib.*, vol. 329, no. 3, pp. 277–288, Feb. 2010.

[91]   J. Loverich, R. Geiger, and J. Frank, "Stiffness nonlinearity as a means for resonance frequency tuning and enhancing mechanical robustness of vibration power harvesters," in *Proceedings of SPIE*, 2008, vol. 6928, p. 692805.

[92]   S. W. Ibrahim and W. G. Ali, "A review on frequency tuning methods for piezoelectric energy harvesting systems," *Journal of Renewable and Sustainable Energy*, vol. 4, no. 6. American Institute of Physics, p. 062703, 13-Nov-2012.

[93]   L. M. Miller, P. Pillatsch, E. Halvorsen, P. K. Wright, E. M. Yeatman, and A. S. Holmes, "Experimental passive self-tuning behavior of a beam resonator with sliding proof mass," *J. Sound Vib.*, vol. 332, no. 26, pp. 7142–7152, 2013.

[94]   L. G. H. Staaf, E. Köhler, M. Soeiro, P. Lundgren, and P. Enoksson, "Smart design selftuning piezoelectric energy harvester intended for gas turbines," *J. Phys. Conf. Ser.*, vol. 660, no. 1, p. 012125, Dec. 2015.

[95]   K. A. Cook-Chennault, N. Thambi, and A. M. Sastry, "Powering MEMS portable devices - A review of non-regenerative and regenerative power supply systems with special emphasis on piezoelectric energy harvesting systems," *Smart Mater. Struct.*, vol. 17, no. 4, p. 043001, Aug. 2008.

[96]   B. S. Lee, W. J. Wu, W. P. Shih, D. Vasic, and F. Costa, "Power harvesting using piezoelectric MEMS generator with interdigital electrodes," in *Proceedings - IEEE Ultrasonics Symposium*, 2007, pp. 1598–1601.

[97]   D. Shen, J. H. Park, J. Ajitsaria, S. Y. Choe, H. C. Wikle, and D. J. Kim, "The design, fabrication and evaluation of a MEMS PZT cantilever with an integrated Si proof mass for vibration energy harvesting," *J. Micromechanics Microengineering*, vol. 18, no. 5, p. 055017, May 2008.

[98]   P. Muralt, M. Marzencki, B. Belgacem, F. Calame, and S. Basrour, "Vibration Energy Harvesting with PZT Micro Device," *Procedia Chem.*, vol. 1, no. 1, pp. 1191–1194, Sep. 2009.

[99]   S.-B. Kim, H. Park, S.-H. Kim, H. C. Wikle, J.-H. Park, and D.-J. Kim, "Comparison of MEMS PZT Cantilevers Based on d_{31} and d_{33} Modes for Vibration Energy Harvesting," *J. Microelectromechanical Syst.*, vol. 22, no. 1, pp. 26–33, Feb. 2013.

[100] J. C. Park, S. Khym, and J. Y. Park, "Micro-fabricated lead zirconate titanate bent cantilever energy harvester with multi-dimensional operation," *Appl. Phys. Lett.*, vol. 102, no. 4, p. 043901, Jan. 2013.

[101] J. Lueke, M. Rezaei, and W. A. Moussa, "Investigation of folded spring structures for vibration-based piezoelectric energy harvesting," *J. Micromechanics Microengineering*, vol. 24, no. 12, p. 125011, Dec. 2014.

[102] H. Yu, J. Zhou, L. Deng, and Z. Wen, "A vibration-based MEMS piezoelectric energy harvester and power conditioning circuit," *Sensors (Switzerland)*, vol. 14, no. 2, pp. 3323–3341, Feb. 2014.

[103] L. Zhang, J. Lu, R. Takei, N. Makimoto, T. Itoh, and T. Kobayashi, "S-shape spring sensor: Sensing specific low-frequency vibration by energy harvesting," *Rev. Sci. Instrum.*, vol. 87, no. 8, p. 085005, Aug. 2016.

[104] G. Zhang, S. Gao, H. Liu, and S. Niu, "A low frequency piezoelectric energy harvester with trapezoidal cantilever beam: theory and experiment," *Microsyst. Technol.*, vol. 23, no. 8, pp. 3457–3466, Aug. 2017.

[105] R. Hosseini and M. Hamedi, "An investigation into resonant frequency of trapezoidal V-shaped cantilever piezoelectric energy harvester," *Microsyst. Technol.*, vol. 22, no. 5, pp. 1127–1134, May 2016.

[106] H. Becker, "Low voltage electrolytic capacitor," *US Pat. 2,800,616*, pp. 2–4, Apr. 1957.

[107] A. Davies and A. Yu, "Material advancements in supercapacitors: From activated carbon to carbon nanotube and graphene," *Can. J. Chem. Eng.*, vol. 89, no. 6, pp. 1342–1357, 2011.

[108]   J. Schindall, "THE CHARGE OF THE Ultra: Capacitors," *IEEE Spectr.*, vol. 44, no. 11, p. 42–46 %U http://search.ebscohost.com.proxy.grenobl, 2007.

[109]   B. E. Conway, "Energy Density and Power Density of Electrical Energy Storage Devices," in *Electrochemical Supercapacitors*, Boston, MA: Springer US, 1999, pp. 417–477.

[110]   B. E. Conway, "Electrochemical Capacitors Based on Pseudocapacitance," in *Electrochemical Supercapacitors*, Boston, MA: Springer US, 1999, pp. 221–257.

[111]   R. A. Fisher, M. R. Watt, and W. Jud Ready, "Functionalized Carbon Nanotube Supercapacitor Electrodes: A Review on Pseudocapacitive Materials," *ECS J. Solid State Sci. Technol.*, vol. 2, no. 10, pp. M3170–M3177, 2013.

[112]   I. Chotia and S. Chowdhury, "Battery storage and hybrid battery supercapacitor storage systems: A comparative critical review," in *Proceedings of the 2015 IEEE Innovative Smart Grid Technologies - Asia, ISGT ASIA 2015*, 2016.

[113]   J. Groot, *State-of-Health Estimation of Li-ion Batteries: Ageing Models*. Chalmers University of Technology, 2014.

[114]   Z. S. Iro, C. Subramani, and S. S. Dash, "A brief review on electrode materials for supercapacitor," *Int. J. Electrochem. Sci.*, vol. 11, no. 12, pp. 10628–10643, 2016.

[115]   W. S. Wang, W. Magnin, and N. Wang, "Supercapacitor and Thin Film Battery Hybrid Energy Storage for Energy Harvesting Applications," *J. Phys. Conf. Ser*, vol. 476, p. 12105, 2013.

[116]   F. Ongaro, S. Saggini, and P. Mattavelli, "Li-Ion Battery-Supercapacitor Hybrid Storage System for a Long Lifetime, Photovoltaic-Based Wireless Sensor Network," *IEEE Trans. Power Electron.*, vol. 27, no. 9, pp. 3944–3952, Sep. 2012.

[117]   J. Kowal, E. Avaroglu, F. Chamekh, A. Šenfelds, T. Thien, D. Wijaya, and D. U. Sauer, "Detailed analysis of the self-discharge of supercapacitors," *J. Power Sources*, vol. 196, no. 1, pp. 573–579, Jan. 2011.

[118]   L. L. Zhang and X. S. Zhao, "Carbon-based materials as supercapacitor electrodes," *Chem. Soc. Rev.*, vol. 38, no. 9, pp. 2520–2531, Aug. 2009.

[119]   D. Qu, "Studies of the activated carbons used in double-layer supercapacitors," *J. Power Sources*, vol. 109, no. 2, pp. 403–411, Jul. 2002.

[120]   A. González, E. Goikolea, J. A. Barrena, and R. Mysyk, "Review on supercapacitors: Technologies and materials," *Renew. Sustain. Energy Rev.*, vol. 58, pp. 1189–1206, May 2016.

[121]   M. Kim, I. Oh, and J. Kim, "Supercapacitive behavior depending on the mesopore size of three-dimensional micro-, meso- and macroporous silicon carbide for supercapacitors," *Phys. Chem. Chem. Phys.*, vol. 17, no. 6, pp. 4424–4433, Jan. 2015.

[122]   Z. S. Wu, Y. Sun, Y. Z. Tan, S. Yang, X. Feng, and K. M??llen, "Three-dimensional graphene-based macro- and mesoporous frameworks for high-performance electrochemical capacitive energy storage," *J. Am. Chem. Soc.*, vol. 134, no. 48, pp. 19532–19535, Dec. 2012.

[123]   N. Liu, J. Shen, and D. Liu, "Activated high specific surface area carbon aerogels for EDLCs," *Microporous Mesoporous Mater.*, vol. 167, pp. 176–181, 2013.

[124]   D. Liu, J. Shen, N. Liu, H. Yang, and A. Du, "Preparation of activated carbon aerogels with hierarchically porous structures for electrical double layer capacitors," *Electrochim. Acta*, vol. 89, pp. 571–576, 2013.

[125]   A. C. Pierre and G. M. Pajonk, "Chemistry of aerogels and their applications," *Chem. Rev.*, vol. 102, no. 11, pp. 4243–4265, 2002.

[126] X. L. Wu, T. Wen, H. L. Guo, S. Yang, X. Wang, and A. W. Xu, "Biomass-derived sponge-like carbonaceous hydrogels and aerogels for supercapacitors," *ACS Nano*, vol. 7, no. 4, pp. 3589–3597, 2013.

[127] Y. Fang, F. Jiang, H. Liu, X. Wu, and Y. Lu, "Free-standing Ni-microfiber-supported carbon nanotube aerogel hybrid electrodes in 3D for high-performance supercapacitors," *RSC Adv.*, vol. 2, no. 16, pp. 6562–6569, 2012.

[128] Z. Gui, H. Zhu, E. Gillette, X. Han, G. W. Rubloff, L. Hu, and S. B. Lee, "Natural cellulose fiber as substrate for supercapacitor," *ACS Nano*, vol. 7, no. 7, pp. 6037–6046, 2013.

[129] J. S. Im, S. W. Woo, M. J. Jung, and Y. S. Lee, "Improved capacitance characteristics of electrospun ACFs by pore size control and vanadium catalyst," *J. Colloid Interface Sci.*, vol. 327, no. 1, pp. 115–119, 2008.

[130] O. Nechyporchuk, M. N. Belgacem, and J. Bras, "Production of cellulose nanofibrils: A review of recent advances," *Industrial Crops and Products*, vol. 93. pp. 2–25, 2016.

[131] A. Greiner and J. H. Wendorff, "Electrospinning: A fascinating method for the preparation of ultrathin fibers," *Angewandte Chemie - International Edition*, vol. 46, no. 30. pp. 5670–5703, 2007.

[132] N. Hedin, V. Sobolev, L. Zhang, Z. Zhu, and H. Fong, "Electrical properties of electrospun carbon nanofibers," in *Journal of Materials Science*, 2011, vol. 46, no. 19, pp. 6453–6456.

[133] J. Fang, H. T. Niu, T. Lin, and X. G. Wang, "Applications of electrospun nanofibers," *Chinese Science Bulletin*, vol. 53, no. 15. pp. 2265–2286, 2008.

[134] K. P. De Jong and J. W. Geus, "Carbon Nanofibers: Catalytic Synthesis and Applications," *Catal. Rev. - Sci. Eng.*, vol. 42, no. 4, pp. 481–510, 2000.

[135] J. Prasek, J. Drbohlavova, J. Chomoucka, J. Hubalek, O. Jasek, V. Adam, and R. Kizek, "Methods for carbon nanotubes synthesis - Review," *J. Mater. Chem.*, vol. 21, no. 40, pp. 15872–15884, Oct. 2011.

[136] M. Sevim, C. Francia, J. Amici, S. Vankova, T. Şener, and Ö. Metin, "Bimetallic MPt (M: Co, Cu, Ni) alloy nanoparticles assembled on reduced graphene oxide as high performance cathode catalysts for rechargable lithium-oxygen batteries," *J. Alloys Compd.*, vol. 683, pp. 231–240, 2016.

[137] R. Reit, J. Nguyen, and W. J. Ready, "Growth time performance dependence of vertically aligned carbon nanotube supercapacitors grown on aluminum substrates," *Electrochim. Acta*, vol. 91, pp. 96–100, 2013.

[138] B. Xu, F. Wu, R. Chen, G. Cao, S. Chen, Z. Zhou, and Y. Yang, "Highly mesoporous and high surface area carbon: A high capacitance electrode material for EDLCs with various electrolytes," *Electrochem. commun.*, vol. 10, no. 5, pp. 795–797, May 2008.

[139] "Sensors Towards Advanced Monitoring and Control of Gas Turbine Engines | Projects | FP7-TRANSPORT | CORDIS | European Commission." [Online]. Available: https://cordis.europa.eu/project/rcn/104300_en.html. [Accessed: 03-Jun-2018].

[140] "gnu.org," .

[141] C. Commons, "Attribution-ShareAlike 3.0 Unported," *URL: http://creativecommons. org/licenses/by-sa/3.0/(la st accessed 07.08. 2012)*, 2007. [Online]. Available: https://creativecommons.org/licenses/by-sa/3.0/. [Accessed: 10-Aug-2018].